Towards Reliable Identification of Diffusion-based Image Manipulations

Alex Costanzino[*] University of Bologna
Woody Bayliss BBC R&D
Juil Sock BBC R&D
Marc Gorriz Blanch BBC R&D
Danijela Horak BBC R&D
Ivan Laptev MBZUAI
Philip Torr University of Oxford
Fabio Pizzati MBZUAI

Abstract

Changing facial expressions, gestures, or background details may dramatically alter the meaning conveyed by an image. Notably, recent advances in diffusion models greatly improve the quality of image manipulation while also opening the door to misuse. Identifying changes made to authentic images, thus, becomes an important task, constantly challenged by new diffusion-based editing tools. To this end, we propose a novel approach for ReliAble iDentification of inpainted AREas (RADAR). RADAR builds on existing foundation models and combines features from different image modalities. It also incorporates an auxiliary contrastive loss that helps to isolate manipulated image patches. We demonstrate these techniques to significantly improve both the accuracy of our method and its generalisation to a large number of diffusion models. To support realistic evaluation, we further introduce BBC-PAIR, a new comprehensive benchmark, with images tampered by 28 diffusion models. Our experiments show that RADAR achieves excellent results, outperforming the state-of-the-art in detecting and localising image edits made by both seen and unseen diffusion models. Further information about our code, data and models, including separate licensing terms, will be publicly available at https://alex-costanzino.github.io/radar/.

1 Introduction

With the advent of diffusion models [21, 15, 69, 52] and associated user-friendly tools [38, 47, 81, 89], image editing has never been so easy and powerful. Along with an unprecedented creative potential, such capabilities also imply risks of misuse. Today, even users with minimal technical expertise can produce highly realistic image edits, raising concerns about the trustworthiness of visual media. In particular, *text-based inpainting methods* [7, 6] can seamlessly insert arbitrary objects into existing scenes. Such edits pose substantial societal threats: for instance, malicious actors could insert compromising elements into a real picture, creating the potential for misinformation, false evidence, or reputational harm [77, 19, 34]. Moreover, removal of certain image elements may aid propaganda or help hide evidence [10]. These safety issues are addressed by approaches for Image Forgery Detection and Localisation (IFDL) [32, 45, 94, 39]. The objective of such methods is to determine whether images have been tampered by editing techniques and to localise modified regions, allowing for the identification of synthetically generated elements.

Given the growing number of image manipulation tools, generalisation of IFDL to the large variety of diffusion models presents a significant challenge. Existing IFDL methods focus mostly on Photoshop-inspired image manipulation – such as copy-pasting visual content – and have limited capabilities

[*]This work was carried out while the author was on a research visit at the University of Oxford.

39th Conference on Neural Information Processing Systems (NeurIPS 2025).

https://doi.org/10.52202/085713-1270

to tackle diffusion-based tampering [39, 45, 32, 94]. We argue that a critical issue is increasingly being overlooked: as the number of available diffusion models for image editing continues to grow, generalisation *across different diffusion models* becomes fundamental. An IFDL model trained on tampered images produced by a single diffusion model may completely fail when encountering images generated by a different model [87]. Given the high realism achieved by diffusion models and the very low barrier to their use – contrary to tools such as Photoshop – we believe there is a need for dedicated solutions *that specifically address robust IFDL for modern diffusion-based tampering*.

Modern IFDL methods often rely on automatically generated tampered images for training [32, 39, 45]. To effectively detect manipulations at test time, it is important to maximise the coverage of image editing models used during training [75]. However, this strategy alone is insufficient as many models remain private, customised, or expensive for large-scale data generation. As a consequence, generalisation to unseen models must be achieved through ad-hoc architectural design choices.

To address the above challenge, we propose RADAR (ReliAble iDentification of inpainted AREas), an IFDL method designed to detect and localise diffusion-based image manipulations in real scenarios. The design of RADAR focuses on two main principles: **(1)** learning effectively from data generated by multiple open-source inpainters, to be robust to a large number of models commonly used for image editing, and **(2)** maximising generalisation to unseen inpainters through targeted architectural choices. For achieving these goals, we propose several contributions. First, we design RADAR's architecture leveraging pre-trained foundation models for feature extraction, capitalising on their generalisation capabilities [56]. Importantly, we enable the use of multiple foundational encoders, capturing both semantic and structural features, which are subsequently fused through a trainable Fusion Block based on cross-attention. This multi-encoder design allows for richer feature representations, improving generalisation and absolute performance. The fused features are then processed by trainable components to extract localisation maps. We then employ a large number of diffusion models during training, maximising the diversity of training data. We impose contrastive constraints on this data, explicitly aligning the feature spaces associated with different inpainters. This enhances RADAR's ability to exploit training data generated with multiple models, along with promoting generalisation.

Finally, to show the need for cross-inpainter IFDL in realistic deployment conditions, we evaluate RADAR and baselines on BBC-PAIR (BBC - Paired Authentic and Inpainted References), a comprehensive benchmark built with 28 different inpainters to reflect real-world inference behaviours. We include three evaluation scenarios in BBC-PAIR, designed to mimic inpainting practices used by users editing images, such as model customisation.

Our contributions can be summarised as follows:

- We develop RADAR, a new method for IFDL designed for cross-inpainter robustness, leveraging multiple foundation models for feature extraction, and transformer-specific contrastive constraints explicitly designed to exploit data generated by multiple inpainters, significantly improving generalisation;
- We propose a novel data generation pipeline and construct BBC-PAIR, a new benchmark for training and evaluating methods for inpainting-based IFDL. BBC-PAIR includes over 150,000 generated images, 28 distinct inpainters, and three evaluation scenarios;
- We demonstrate state-of-the-art performances on all three BBC-PAIR scenarios, against 7 recent baselines, for both detection and localisation of tampered areas.

2 Related work

Identifying synthetic images. Many methods have been developed to identify synthetic images [20, 13, 57, 80, 28, 83, 91, 23] without abilities to localise tampered regions. Instead, IFDL methods identify both tampered images and localised regions generated by diffusion models. The problem is typically addressed as a data-driven task, although there also exist training-free approaches [92, 66]. Some rely on the RGB modality only [63], while many [33, 32, 94, 46, 78, 18] employ low-level multi-modal fused features from spatial and frequency domains, to raise sensitivity to splicing and copy-move across images. This requires training of ad-hoc encoders, limiting generalisation. SAFIRE [45] uses foundation models, but still focuses on a single modality. Others [39, 86, 85] propose language model-based approaches, limited in scale as they require human-verified labels. RADAR instead

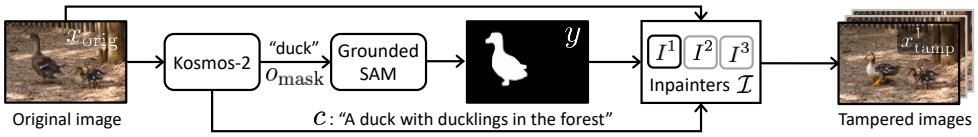


Figure 1: **Data generation pipeline.** We first extract with Kosmos-2 [58] a set of objects in an image x_{orig}, along with a caption c. We then use Grounded SAM [65] to segment one of the objects o_{mask} (e.g. "duck"). Lastly, we use a set of K text-to-image inpainters $\mathcal{I}$ to generate K tampered images $\{x^k_{\text{tamp}}\}_{k=1}^K$. We use c as a prompt to avoid the generation of objects irrelevant to the scene.

can be trained with automatically-generated data, and exploits multiple pre-trained foundational transformers, extracting variate sets of high-level features, ultimately benefiting performance.

Generalisation in image forensics. Diversity of data helps generalisation [71, 35], although the effects of distributional biases remain significant even for large-scale training [3]. This justifies the combination of large-scale training and generalisation techniques. In deepfake detection, this problem has been tackled, either by increasing the number of models used for data generation [25, 57] or with pipelines based on foundation models [54, 74]. In IDFL, instead, many approaches train on data generated by a restricted set of inpainters, limiting cross-model generalisability [32, 39, 45, 94, 18]. While some use contrastive learning for generalisation [45, 17], we exploit a novel transformer-specific contrastive strategy on patch representations, designed by reasoning about different distributions emerging while editing images with diffusion models.

Evaluation of IFDL. Benchmarks for image forensics have evolved together with the progress in tools for image manipulation. Initial efforts focused on splicing detection, with the Columbia [37], VIPP [8], and DSO-1 [12] datasets. The field then expanded with CASIA [24] and NIST16 [31], which incorporated diverse manipulation types including splicing, copy-move, and removal attacks, while COVERAGE [84] specifically targeted copy-move detection through semantically challenging examples. The advent of diffusion models made necessary a new generation of benchmarks [53, 32, 45, 39]: CocoGlide [32] introduced the first evaluation of diffusion-based inpainting artifacts, while only recently Safire-MS Expert [45] and SID-Set [39] addressed the broader challenges of detecting and localizing synthetic content across varying scales and model architectures. However, these benchmarks rely on a single inpainting model for image generation. Larger-scale efforts either focus on synthetic image detection only [36, 57, 87], or include a limited set of inpainters [18]. In contrast, our BBC-PAIR spans images modified by 28 inpainters from open source, LoRA-customised, and closed source, to effectively assess generalisation capabilities in realistic setups.

3 RADAR

We aim to identify a pixel-wise map of regions inpainted by a diffusion model on an input image x. We first generate training data suitable for the task with multiple inpainters, as shown in Figure 1 (Section 3.1). As illustrated in Figure 2, our model RADAR obtains patch features for input images using transformer-based foundation models (Section 3.2). This allows RADAR to benefit from the generalisation capabilities of foundation models, whilst capturing image tampering cues from multiple modalities. We fuse modality-specific representations with a custom attention-based Fusion Block (Section 3.2). In addition, to improve generalisation across inpainters, we exploit ad hoc contrastive constraints during training (Section 3.3). Finally, we produce a tampering map $\tilde{y}$ with a Localisation Head which is trained using our automatically generated dataset (Section 3.4). At inference, besides localising modified image regions $\tilde{y}$, we also aggregate pixel-wise predictions to compute a detection score, predicting whether the image has been tampered or not.

3.1 Data generation

Similar to other works [45, 32], we design an ad-hoc data generation pipeline, shown in Figure 1. We begin by sampling an image $x_{\text{orig}} \sim \mathcal{D}_{\text{orig}}$ from a dataset $\mathcal{D}_{\text{orig}}$, which contains only genuine images. The image x_{orig} is processed with the Kosmos-2 [58] multi-modal language model, prompted to extract a list of object names present in the scene, denoted as $\mathcal{O}_x = \{o^1, o^2, \ldots, o^n\}$, and a

https://doi.org/10.52202/085713-1270

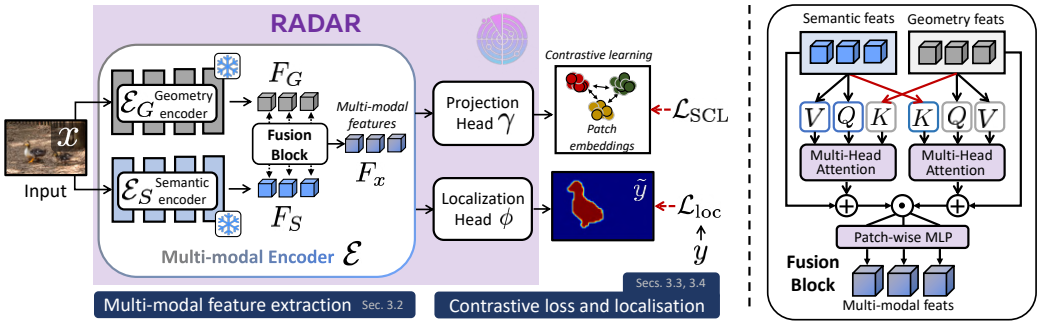


Figure 2: **Training RADAR.** We first extract, for an input image x, multi-modal features F_x by using our multi-modal encoder $\mathcal{E}$. To implement $\mathcal{E}$, we employ the pre-trained Semantic Encoder $\mathcal{E}_S$ and Geometry Encoder $\mathcal{E}_G$, and fuse their extracted features with a Fusion Block (on the right, in details). The Fusion Block exploits a symmetric cross-attention mechanism, based on the swapping of keys K in two multi-head attention mechanisms. For fusion, we use a patch-wise MLP. We process the resulting multi-modal features with a Localisation Head ϕ, mapping to tampering maps $\tilde{y}$. Using $\tilde{y}$ and y, we back-propagate a localisation loss $\mathcal{L}_{\text{loc}}$. To increase generalisation across inpainters, we use a Projection Head γ to extract embeddings on which we impose a contrastive loss $\mathcal{L}_{\text{SCL}}$.

caption c describing the scene. For each image, we randomly sample an object name $o_{\text{mask}} \sim \mathcal{O}_x$ (e.g. "duck") from the set. The selected object name o_{mask} is used as a prompt for Grounded SAM [65] (GS), which extracts a semantic mask of the object. We define a tampering mask y as the mask extracted by GS, *i.e.* $\text{GS}(x_{\text{orig}}, o_{\text{mask}})$. Then, we consider a set of K text-based inpainters $\mathcal{I} = \{I^1, I^2, \ldots, I^K\}$. For a given pair (x_{orig}, y), we apply each inpainter $I^k \in \mathcal{I}$ to obtain a tampered image $x^k_{\text{tamp}} = I^k(x_{\text{orig}}, y, c)$, where c is the previously extracted caption, used as an inpainting prompt. This ensures that the inpainter generates plausible objects, increasing contextual coherence. For instance, in Figure 1, inpainting an aeroplane rather than a duck would impact realism. We also randomly replace y with an algorithmically-generated mask to reduce semantic biases. More details in the Appendix.

For each original image $x \in \mathcal{D}_{\text{orig}}$ we construct a sample $\mathcal{X} = \{x_{\text{orig}}, x^1_{\text{tamp}}, x^2_{\text{tamp}}, \ldots, x^K_{\text{tamp}}, y\}$. By processing every $x \in \mathcal{D}_{\text{orig}}$ in this way, we obtain a dataset $\mathcal{D} = \bigcup_{x \in \mathcal{D}_{\text{orig}}} \mathcal{X}$ including original samples, the corresponding tampered images, and ground-truth masks.

3.2 Foundation models as feature extractors

Multi-modal cues. We build on the generalisation capabilities of foundational models [56] and extract image features using pre-trained visual encoders. Rather than using a single encoder, we fuse representations obtained from *two different models* focused on semantic and geometric image understanding. Manipulations may indeed exhibit semantic inconsistencies, such as incoherent textures, requiring adequate semantic-rich feature extraction for identification [49]. However, tampered regions may also reveal structural inconsistencies, such as violations of 3D coherence [70], making it identifiable only with a correct geometric interpretation of the scene. Importantly, these signals may not point to any single artefact, but emerge only when reasoning about the scene as a whole.

Following this, we define two pre-trained encoders for feature extraction. First, we employ a *Semantic Encoder* $\mathcal{E}_S$, *i.e.* a network trained to extract semantically rich features. Since self-supervised learning has been shown to promote the emergence of meaningful semantic representations [16], we adopt DINO-v2 [56] for $\mathcal{E}_S$. In parallel, to capture structural cues, we introduce a *Geometry Encoder* $\mathcal{E}_G$. Here, we use Depth Anything V2 encoder [88], which is well suited to extracting geometry-oriented features thanks to its large-scale pretraining for depth estimation. This choice of modalities is also inspired by relevant works [79, 29, 93]. Notably, both encoders share the same transformer backbone, making their embedding spaces naturally compatible for fusion, yet capturing different features.

In practice, we forward an input x to both encoders, yielding $F_S = \mathcal{E}_S(x), F_G = \mathcal{E}_G(x)$. F_S and F_G refer to sequences of N patch-based features extracted by the transformer encoders, so

https://doi.org/10.52202/085713-1270

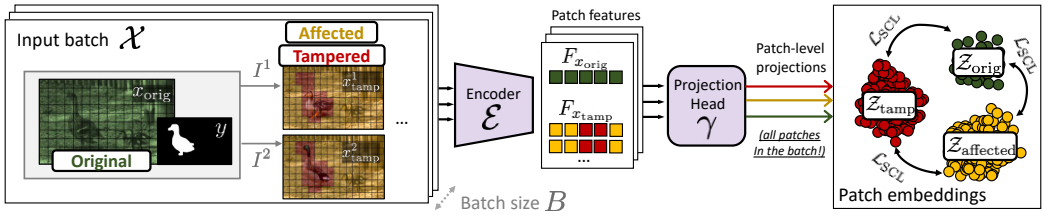


Figure 3: **Contrastive learning.** We identify **original**, **tampered** and **affected** patches. Corresponding feature patches are mapped by the head γ to $\mathcal{Z}$ embeddings, on which we impose the contrastive loss $\mathcal{L}_{\text{SCL}}$, enforcing patch features of the same distribution to be clustered together. Note that we aggregate $\mathcal{Z}$ embeddings from multiple inpainters, promoting cross-inpainter generalisation.

$F_S = \{f_S\}_{n=1}^{N}, F_G = \{f_G\}_{n=1}^{N}$, with f_G and f_S being the individual patch-level features of each encoder, shown in Figure 2.

Fusion block. For multi-modal processing, we need to combine two sets of features. Inspired by previous works [76, 14], we fuse the patch-level features extracted by both encoders with a symmetric cross-attention mechanism. Intuitively, this compensates for the lack of information in each modality by attending to relevant visual cues in the other modality. We implement this using Multi-Head Attention (MH) layers, where we combine the keys K of one modality with the queries Q and values V of the other, as shown in Figure 2 (right):

$$F_{S\leftarrow G} = \text{MH}_{\text{S}\leftarrow\text{G}}\left(K(F_S), Q(F_G), V(F_G)\right) \quad F_{G\leftarrow S} = \text{MH}_{G\leftarrow\text{S}}\left(K(F_G), Q(F_S), V(F_S)\right). \quad (1)$$

The $K(\cdot), Q(\cdot)$ and $V(\cdot)$ operators are implemented as multi-layer perceptrons (MLPs), separately for each modality. Then, we use another MLP to fuse information about corresponding features at the patch level. The MLP processes each pair of patches separately, hence being a *patchwise MLP* (Figure 2). We share the MLP weights across all pairs. A patch feature f_M in the sequence is:

$$f'_S = f_S + f_{S\leftarrow G}, \quad f'_G = f_G + f_{G\leftarrow S}, \quad f_M = \text{MLP}\left([f'_S, f'_G]\right), \quad (2)$$

where $[\cdot]$ denotes concatenation. We set up the MLP so that f_M has the same dimensionality as f_S and f_G. We obtain F_x by aggregating processed patches, $F_x = \{f_M\}_{n=1}^{N} = \mathcal{E}(x)$, abstracting our multi-modal feature extraction as $\mathcal{E}$.

3.3 Patch-level contrastive learning

Contrastive distributions. As mentioned in Section 3.1, for each x_{orig} we generate multiple $\{x^1_{\text{tamp}}, ..., x^K_{\text{tamp}}\}$, with different models. Training on data from multiple models helps generalising in deepfake detection [57], but we experienced that naively using more inpainters for a fine-grained task, such as forgery localisation, leads to suboptimal performance. To mitigate this, we use contrastive learning. Intuitively, we aim to map features extracted from patches tampered by different models to a unique **tampered** distribution, and maximise their separation from an **original** distribution of untampered patches. Doing so, we encourage RADAR to focus on common characteristics *across diffusion models*, helping to exploit variable data. Importantly, this also aids generalisation to unseen models.

During each training iteration we sample a batch of B samples $\{\mathcal{X}^1, \mathcal{X}^2, \ldots, \mathcal{X}^B\}$, where $\mathcal{X}^b \sim \mathcal{D}$, $b \in [1, B]$. For each tampered x^k_{tamp} in the batch, we extract the indices of **tampered** patches, *i.e.* those that overlap with the inpainting mask. Likewise, we extract all patch indices from the original image as a representation of a **original** distribution. In Figure 3, we show how we classify patches following this definition. For clarity, we define $\mathcal{P}(x)$ as the set of patch indices corresponding to the patch grid of image x. That is, $\mathcal{P}(x)$ returns all patches spatially tiled over x, patch indices in the batch are defined as:

$$\mathcal{P}_{\text{tamp}} = \bigcup_{b=1}^{B}\bigcup_{k=1}^{K}\{p \in \mathcal{P}(x^{b,k}_{\text{tamp}}) | \sum_{i\in p} y^b_i > 0\}, \quad \mathcal{P}_{\text{orig}} = \bigcup_{b=1}^{B}\left\{p \in \mathcal{P}(x^b_{\text{orig}})\right\}, \quad (3)$$

where $i \in p$ denotes all pixel indices within patch p, and y_i is the value of the mask at pixel i.

https://doi.org/10.52202/085713-1270

Empirically, we find it beneficial to model a third category of patches, which we refer to as **affected**. These patches originate from tampered images but *do not overlap* with the inpainting mask, as we show in Figure 3 in yellow. Despite not being directly manipulated, such patches exhibit distributional shifts due to the auto-encoding process in latent diffusion models [68], which constitute the vast majority of open models. Hence, we define:

$$\mathcal{P}_{\text{affected}} = \bigcup_{b=1}^{B} \bigcup_{k=1}^{K} \{p \in \mathcal{P}(x_{\text{tamp}}^{b,k}) | \sum_{i \in p} y_i^b = 0\}. \tag{4}$$

Contrastive constraint for transformers. Next, we aim to separate distributions of the extracted patch features using a contrastive objective. We process the same batch of samples $\{\mathcal{X}^1, \ldots, \mathcal{X}^B\}$ following the multi-modal encoding described in Sec. 3.2, projecting the extracted patch-level features into a contrastive embedding space to enable distribution-level discrimination. For each image x in the batch, where x refers to either x_{orig} or any tampered x_{tamp}^k, we compute its representation $F_x = \mathcal{E}(x) = \{f_M\}_{k=1}^N$. Each patch feature $f_M \in F_x$ is then forwarded to a Projection Head γ, implemented as a patch-wise MLP as before, yielding projected embeddings Z_x that we can aggregate into a feature set $\mathcal{Z}$:

$$Z_x = \{\gamma(f_M)\}_{n=1}^N = \{z\}_{n=1}^N, \quad \mathcal{Z} = \bigcup_{b=1}^{B} \bigcup_{x \in \mathcal{X}^b} Z_x. \tag{5}$$

We write $\{z\}_{p \in \mathcal{P}}$ to denote the set of patch-level embeddings whose indices are in $\mathcal{P}$, and collect projected features associated with the patch index sets defined earlier:

$$\mathcal{Z}_{\text{orig}} = \{z\}_{p \in \mathcal{P}_{\text{orig}}}, \quad \mathcal{Z}_{\text{tamp}} = \{z\}_{p \in \mathcal{P}_{\text{tamp}}}, \quad \mathcal{Z}_{\text{affected}} = \{z\}_{p \in \mathcal{P}_{\text{affected}}}. \tag{6}$$

Ideally, as depicted in Figure 3, we would like each set of features to be well clustered, maximising its distance from others. This will ease the identification of affected patches [42]. We then enforce a supervised contrastive loss [43], treating each group as a distinct class. Let $\ell_z \in \{\texttt{orig}, \texttt{tamp}, \texttt{affected}\}$ denote the label associated with embedding $z \in \mathcal{Z}$. For each anchor $z_i \in \mathcal{Z}$, we define its anchor group $\mathcal{A}_i$:

$$\mathcal{A}_i = \{z_j \in \mathcal{Z} \setminus \{z_i\} \mid \ell_j = \ell_i\}, \tag{7}$$

and minimize the contrastive objective $\mathcal{L}_{\text{SCL}}$:

$$\mathcal{L}_{\text{SCL}} = \sum_{z_i \in \mathcal{Z}} -\frac{1}{|\mathcal{A}_i|} \sum_{z_j \in \mathcal{A}_i} \log \frac{\exp\left(z_i^\top z_j\right)}{\sum_{z_k \in \mathcal{Z} \setminus \{z_i\}} \exp\left(z_i^\top z_k\right)}. \tag{8}$$

Importantly, our contrastive learning imposes separation or aggregation on patch representations, hence *naturally exploiting transformer-based encoding*.

3.4 Localising tampering

Training. We aim to estimate tampering maps from input images. For simplicity, let us consider a single training sample $\mathcal{X} = \{x_{\text{orig}}, x_{\text{tamp}}^1, \ldots, x_{\text{tamp}}^K, y\}$. For each image $x \in \mathcal{X}$, we process the extracted multi-modal features $F_x = \mathcal{E}(x)$ through a Localisation Head ϕ, implemented as a convolution followed by a sigmoid activation, following common practices in feature probing [11, 56]. This yields a tampering score map $\tilde{y} = \phi(F_x)$, as shown in Figure 2. At training time, we use both x_{orig} and all x_{tamp}, defining a supervision mask y_{train} based on whether x is tampered or not, hence $y_{\text{train}} = y$ if $x \neq x_{\text{orig}}$, and $y_{\text{train}} = \mathbf{0}$ otherwise. We then define the localisation loss as the sum of a binary cross-entropy loss and a dice loss [73]:

$$\mathcal{L}_{\text{loc}}(x) = \mathcal{L}_{\text{BCE}}(\tilde{y}, y_{\text{train}}(x)) + \mathcal{L}_{\text{dice}}(\tilde{y}, y_{\text{train}}(x)). \tag{9}$$

Assuming a batched training, we can now impose our full objective:

$$\mathcal{L} = \mathcal{L}_{\text{SCL}} + \sum_{b=1}^{B} \sum_{x \in \mathcal{X}^b} \mathcal{L}_{\text{loc}}(x, y_{\text{train}}(x)). \tag{10}$$

Table 1: **Quantitative comparison.** We compare the three different setups of BBC-PAIR, *always significantly outperforming all other baselines*. As expected, we perform best on the ID set. Performance is also robust to the LoRA set, showing generalisation to customised models. In the presence of completely unseen inpainters (OOD), RADAR is still robust enough to outperform all competitors.

Method	BBC-PAIR-ID				BBC-PAIR-LoRA				BBC-PAIR-OOD			
	Det.		Loc.		Det.		Loc.		Det.		Loc.	
	AUC↑	Acc↑	F1↑	IoU↑	AUC↑	Acc↑	F1↑	IoU↑	AUC↑	Acc↑	F1↑	IoU↑
HiFi-Net [33]	0.625	0.509	0.750	0.376	0.650	0.503	0.732	0.365	0.574	0.525	0.689	0.382
TruFor [32]	0.548	0.538	0.739	0.434	0.519	0.529	0.765	0.443	0.610	0.580	0.752	0.437
MIML [63]	0.468	0.483	0.214	0.110	0.517	0.500	0.240	0.131	0.629	0.505	0.187	0.098
AdaIFL [48]	0.533	0.498	0.762	0.383	0.540	0.532	0.763	0.412	0.606	0.554	**0.791**	0.447
Mesorch [94]	0.581	0.560	0.744	0.402	0.560	0.519	0.758	0.398	0.667	0.610	0.790	0.441
SAFIRE [45]	0.594	0.531	0.668	0.375	0.515	0.515	0.673	0.395	0.593	0.507	0.716	0.439
SIDA [39]	0.598	0.598	0.764	0.536	0.554	0.554	0.680	0.508	0.679	0.679	0.721	0.425
RADAR	**0.945**	**0.931**	**0.832**	**0.600**	**0.901**	**0.773**	**0.810**	**0.521**	**0.805**	**0.709**	0.785	**0.450**

During training, we back-propagate the total loss $\mathcal{L}$ to optimise the Localisation Head ϕ, the Projection Head γ, and the Fusion Block, while keeping the multi-modal encoders frozen to preserve the modality-specific features they encode. Notably, since our contrastive strategy operates at the patch level, a batch yields a large number of samples in each $\mathcal{Z}$. This naturally benefits contrastive learning, which is known to improve with larger sets of comparisons [43].

Inference. At inference time, we discard γ and use the Localisation Head ϕ to obtain a pixel-wise tampering probability $\tilde{y}$, which we binarise to produce tampering maps. Akin to others [22, 90], we define the probability of an entire image to be tampered as the mean of the top 1% highest values within $\tilde{y}$. This focuses on the most prominent forgery-related features while reducing the influence of low-confidence regions. We binarise this value with a threshold 0.5 to perform detection of tampered images.

4 Experiments

4.1 Setup

BBC-PAIR We use Section 3.1 to create the BBC-PAIR benchmark, allowing us to evaluate RADAR and baselines in three different setups. For each setup, we also include the original images x_{orig} to evaluate performance in the absence of tampering. Note that BBC-PAIR also includes existing benchmarks.

BBC-PAIR-ID We consider 15,000/100 randomly sampled OpenImages-v7 [50] as $\mathcal{D}_{\text{orig}}$ for train/test, and we use the data generation pipeline in Section 3.1 with 10 inpainters in $\mathcal{I}$: Stable Diffusion (SD) versions 1.4/1.5/2.1 [68], SD 3/3.5 [26], SDXL [62], Kandinsky 2.2 [64] and 3.1 [5], FLUX.1 [9] `schnell` and `dev`. All models are latent [68] and use Diffusers [61] inpainting pipelines, with parameters reported in the Appendix. We generate 150,000/1,000 images for training/testing, processing each image in $\mathcal{D}_{\text{orig}}$ with all $I \in \mathcal{I}$. Training on this set, we will be in-distribution (ID) for these inpainters.

BBC-PAIR-LoRA We edit the x_{orig} in the test split of BBC-PAIR-ID with 10 LoRAs, applied to SD1.5 [68], SD3.5 [26], SDXL [62] and FLUX.1 [9], generating 500 images. We report the LoRAs in the Appendix. Since we apply LoRAs to the inpainters of the ID set, this BBC-PAIR-LoRA set allows us to measure the effects of the model customisation on RADAR.

BBC-PAIR-OOD To evaluate cross-inpainter generalisation, we synthesise data using *completely unseen* inpainters, hence having maximum distribution shift w.r.t. BBC-PAIR-ID. First, we generate 750 tampered images with 8 commercial inpainters: ClipDrop [72], Dall-E 2 [55], Adobe Firefly [1], FLUX.1 Fill [pro] [27], Ideogram [40], LightX [4], Phot.AI [60], YouCam [59]. We use DIV2K [2] as $\mathcal{D}_{\text{orig}}$ to maximise differentiation with the ID set. OOD evaluation also implies testing in uncontrolled scenarios. So, we select the existing inpainting-based CocoGlide [32], SafireMS-Expert [45] and SID-Set [39] test sets, to evaluate robustness to inpainting strategies different from ours. The union

https://doi.org/10.52202/085713-1270

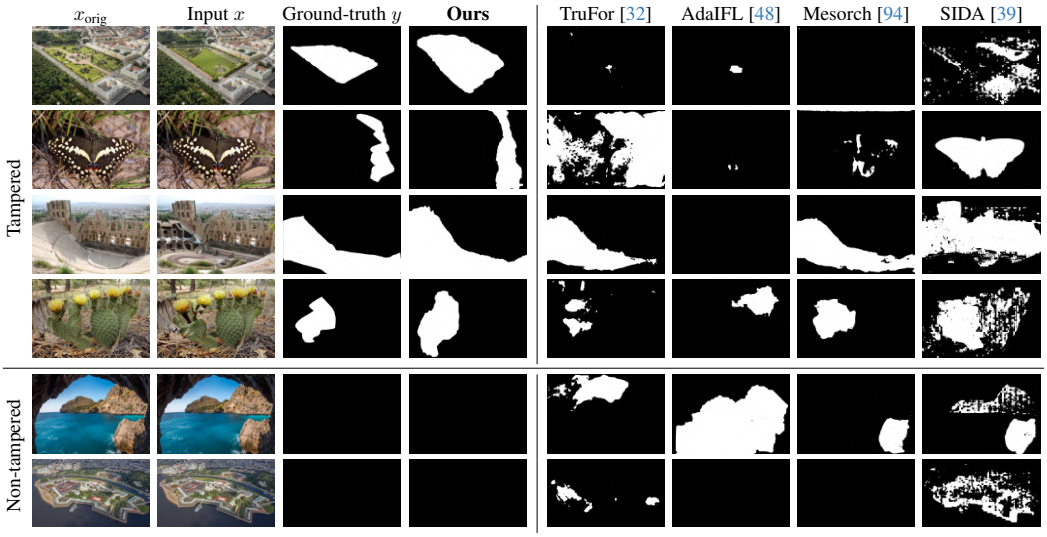


Figure 4: **Qualitative results.** Compared to the best baselines in the OOD scenario, RADAR accurately localises tampering. Baselines exhibit semantic biases, as SIDA (second row) and Mesorch (fifth row) identify full objects. Importantly, RADAR is robust to false positives and does not react to non-tampered images (last two rows). This explains our superior performance in detection.

of these samples is BBC-PAIR-OOD. *Detailed performance evaluation of all included datasets is in the Appendix*. We report only the average in the main paper due to space constraints.

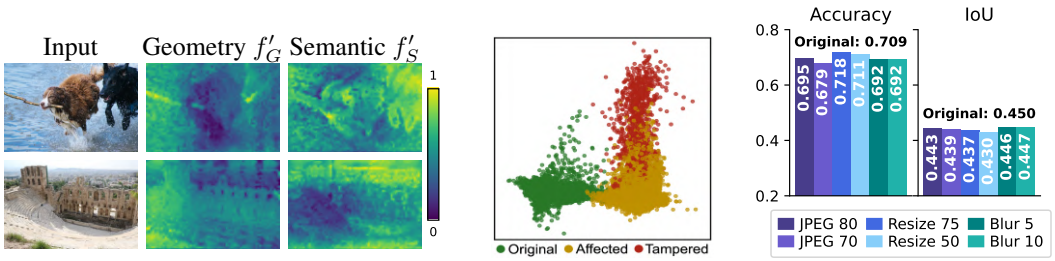
Baselines and metrics. We exhaustively compare against the best recent open source methods: TruFor [32], HiFi-Net [33], SAFIRE [45], Mesorch [94], MIML [63], AdaIFL [48] and SIDA [39]. For localisation, we employ F1 and IoU to evaluate the similarity with the ground truth mask y, as commonly reported [39, 32, 45, 48]. Note that localisation is only evaluated on tampered images, akin to well-established practices [32, 39, 45, 94]. Consistent with recent studies [39, 32, 33, 94], we also evaluate on binary detection performances, using the area under the ROC curve (AUC) and accuracy with threshold 0.5 to evaluate the classification of images as tampered or not (Section 3.4). Since AdaIFL and MIML do not natively support forgery detection, we calculate a detection score as ours, selecting the most confident values of the tampering map $\tilde{y}$ (Section 3.4).

Training details. We train RADAR for 120 epochs with batch-size 16, dropout ($p = 0.1$) and NAdam optimiser [44] (`lr`=10^{-4} and decay of 10^{-5}) using 4 NVIDIA A100 80GB GPUs, optimizing the fusion block, γ and ϕ while keeping $\mathcal{E}_S$ and $\mathcal{E}_G$ frozen. More details are given in the Appendix.

4.2 Comparisons with baselines

Table 1 reports experimental comparison with baselines. We *significantly outperform all methods* in both detection and localisation. As expected, we yield the highest metrics in the ID set. Note that while we have an advantage against baselines on ID data – since our training data are generated by the same inpainters – this allows us to be more robust in realistic scenarios. For the deployment of RADAR, *we aim to maximise performance on inpainters commonly used for image editing*, such as open source models. Since open source models allow data generation with ease, we argue that the best practice is to use them for training. Most importantly, RADAR also shines in generalisation, yielding the best localisation on both LoRA (**0.521** in IoU) and OOD sets (**0.450** in IoU).

Interestingly, in detection, all baselines suffer considerably, yielding low accuracies. We attribute this to their limited robustness to the distribution shift with respect to their training data. The better generalisation of RADAR, instead, is reflected in *highly superior detection performance*, improving AUC **+0.32**/**+0.25**/**+0.13** against the second best for ID/LoRA/OOD. We report detailed performance tables in the Appendix, including separate evaluations on each of the BBC-PAIR-OOD datasets. Since localisation performance is evaluated on tampered images only – following well-established practices [39, 32, 45, 94] – detection results *assess our robustness to false positives*. This is noticeable



(a) Multi-modal activations (b) UMAP analysis (c) Robustness to perturbations

Figure 5: **Properties of RADAR.** In Figure (a), we analyse feature magnitude in both encoders $\mathcal{E}_S$ and $\mathcal{E}_G$, highlighting that they are roughly complementary. In Figure (b), we show with UMAP [51] that **affected** patches serve as separators between **original** and **tampered**, justifying our boost in performance. In Figure (c), we demonstrate robustness to common web image operations, namely JPEG compression, resizing, and Gaussian blur.

in the qualitative results in Figure 4 on the BBC-PAIR-OOD set. Not only does RADAR produce more accurate masks to identify tampered regions, but it also correctly ignores non-tampered images (last two rows), where baselines produce predictions on objects in the scene instead (as the rock). SIDA also exhibits semantic biases (second row), identifying full objects as fake (the butterfly). This makes RADAR predictions more reliable for deployment, satisfying our initial design requirements. Note that we provide more qualitative and detailed comparisons in the Appendix.

4.3 Properties of RADAR

Next, we investigate some emerging properties of RADAR. For our investigation, we use the BBC-PAIR-OOD test set to minimise the distribution bias in the observed behaviour of the network.

Multi-modality. We display in Figure 5a the normalised activations of f'_G and f'_S in Equation (2) (hence, the features before fusion), averaged over channels for tampered inputs. Each map represents the importance of the features of each modality, per pixel, and ranges from 0 (low importance) to 1 (high importance). We notice that the spatial distribution of activations is roughly complementary across modalities. In other words, it shows that $\mathcal{E}_G$ and $\mathcal{E}_S$ tend to consider different elements for their feature extraction. This proves that our design choices, based on semantic and geometric encoders, allow us to extract meaningful features for the entirety of the scene, visually showing the reasons behind RADAR's performance. Interestingly, while semantic features focus on subjects (such as the dogs in the first row), geometric features highlight regular structures (such as the stairs in the second row). We conjecture that this may aid in detecting different types of tampering.

Distribution analysis. We want to understand the role of **affected** patches in the $\mathcal{L}_{\text{SCL}}$ optimisation. In Figure 5b, we report a UMAP [51] plot of the patch-level projection features extracted by γ on BBC-PAIR-OOD. We observe that **affected** patches separate **original** and **tampered** clusters. This highlights that the hybrid nature of the **affected** patch distribution, processed by the auto-encoder in latent diffusion models, while containing no generated content, *naturally emerges during training* as an intermediate distribution, justifying our design.

Robustness to perturbations. In Figure 5c, we study RADAR performance in terms of Accuracy (detection) and IoU (localisation) on BBC-PAIR-OOD with common perturbations introduced by the upload on the web, such as JPEG compression (80/70 rate), resizing (75%/50%), or blurring with a Gaussian filter (variance 10/5). We highlight *negligible performance drops* in all tasks, further proving RADAR's robustness. We attribute this to the large pre-training of $\mathcal{E}_S$ and $\mathcal{E}_G$, presumably including perturbed images as well and consequently inducing robustness to perturbations in RADAR.

4.4 Ablation studies

We now present ablation studies on our contributions. Due to RADAR's training cost, for the following experiments, we train on 10% of the original BBC-PAIR-ID for 70 epochs.

https://doi.org/10.52202/085713-1270

Table 2: **Ablation studies.** We investigate fusion strategies, contrastive formulations, and the number of inpainters (K). Our setup is always the best.

Setup	BBC-PAIR-ID				BBC-PAIR-LoRA				BBC-PAIR-OOD			
	Det.		Loc.		Det.		Loc.		Det.		Loc.	
	AUC↑	Acc.↑	F1↑	IoU↑	AUC↑	Acc.↑	F1↑	IoU↑	AUC↑	Acc.↑	F1↑	IoU↑
Multi-modality and fusion												
$\mathcal{E}_S$ only	0.582	0.502	0.780	0.538	0.590	0.510	0.735	0.484	0.567	0.516	0.706	0.410
$\mathcal{E}_G$ only	0.589	0.541	0.781	0.533	0.558	0.502	0.774	0.496	0.524	0.510	0.736	0.422
Concat	0.691	0.529	0.788	0.546	0.581	0.515	0.773	**0.498**	0.543	0.519	0.748	**0.427**
Sum	0.602	0.515	0.785	0.538	0.598	0.510	0.756	0.484	0.523	0.513	0.739	**0.427**
Ours	**0.921**	**0.893**	**0.790**	**0.547**	**0.771**	**0.678**	**0.789**	0.474	**0.746**	**0.689**	**0.773**	0.422
Contrastive Learning												
w/o $\mathcal{L}_{\text{SCL}}$	0.903	0.849	0.774	0.511	0.627	0.599	0.743	0.424	0.709	0.670	0.718	0.402
w/o Affect.	**0.932**	0.872	**0.790**	**0.550**	0.763	**0.694**	0.777	0.465	0.729	0.676	0.756	0.423
Affect=Orig	0.922	0.856	0.783	0.538	0.727	0.651	0.771	0.447	0.741	0.688	0.758	**0.428**
Ours	0.921	**0.893**	**0.790**	0.547	**0.771**	0.678	**0.789**	**0.474**	**0.746**	**0.689**	**0.773**	0.422
Number of inpainters K												
$K = 1$	0.896	0.793	0.804	0.485	0.692	0.582	0.766	0.406	0.720	0.623	**0.809**	**0.425**
$K = 5$	**0.937**	0.858	**0.811**	0.524	0.763	0.625	0.774	0.423	0.741	0.636	0.794	0.421
$K = 10$ **(Ours)**	0.921	**0.893**	0.790	**0.547**	**0.771**	**0.678**	**0.789**	**0.474**	**0.746**	**0.689**	0.773	0.422

Fusion Block. We evaluate the architecture of our multimodal encoder in Table 2 (top). We first restrict the model to single encoders ($\mathcal{E}_S$ and $\mathcal{E}_G$ only), and observe *significant decrease in performance*, highlighting the importance of complementary encoders used by RADAR. This shows that both semantic and geometric cues are fundamental for a proper understanding of the scene in IFDL. We also investigate simpler fusion mechanisms, replacing the multi-head attention with simple Concat or Sum operations followed by an MLP. In all cases, performance drops significantly, especially for detection (AUC **0.921** vs. **0.691** and Acc. **0.893** vs. **0.541** of the best alternative). This shows that our Fusion Block is important for extracting meaningful cues from heterogeneous foundation models.

Contrastive loss. We investigate alternative setups of our contrastive formulation in Table 2 (middle). Removing $\mathcal{L}_{\text{SCL}}$ (w/o $\mathcal{L}_{\text{SCL}}$) yields the highest drop in performance (AUC **0.932** vs. **0.921** and Acc. **0.893** vs. **0.849** in detection, F1 **0.790** vs. **0.774** and IoU **0.550** vs. **0.511** in localisation), showing that only expanding $\mathcal{I}$ is suboptimal. We also investigate the effectiveness of the **affected** distribution, first removing it completely (w/o affected) and then mapping **affected** patches to the **original** class instead (Affect=Orig, see Section 3.3). All alternative configurations result in worse performance.

Number of inpainters. We test RADAR by reducing the number of inpainters K in $\mathcal{I}$ used for training. We compare training with $K = \{1, 5, 10 \text{ (ours)}\}$ by randomly selecting K inpainters over the full set of 10 inpainters used for the generation of BBC-PAIR-ID. We normalise the computational cost for training, and report the average over 3 runs in Table 2 (bottom). For both detection and localisation, increasing the number of inpainters *significantly boosts results* (Acc. **0.893** vs. **0.793** in detection, IoU **0.547** vs. **0.485** in localisation).

5 Conclusions

We introduced RADAR, a novel IFDL method designed to maximise in-distribution coverage and generalisation to unseen diffusion models. We proposed architectural contributions, fusing features extracted by multiple foundation models, and exploiting transformer-specific contrastive constraints on extracted patch features to promote generalisation. We also introduce BBC-PAIR, for a fair assessment in the presence of open-source models, model customisation, and commercial solutions. While we significantly outperform the state-of-the-art in IFDL, we emphasise that the complexity of the problem still leaves room for improvement. We hope that our research will encourage future work in this direction to mitigate the potential high societal impact of image manipulations.

References

[1] Adobe Inc.: Adobe firefly. https://firefly.adobe.com (2023)

[2] Agustsson, E., Timofte, R.: Ntire 2017 challenge on single image super-resolution: Dataset and study. In: IEEE Conference on Computer Vision and Pattern Recognition Workshops (2017)

[3] Al Kader Hammoud, H.A., Das, T., Pizzati, F., Torr, P.H., Bibi, A., Ghanem, B.: On pretraining data diversity for self-supervised learning. In: European Conference on Computer Vision (2024)

[4] AndOr Communications Pvt Ltd: Lightx. https://www.lightxeditor.com (2016)

[5] Arkhipkin, V., Vasilev, V., Filatov, A., Pavlov, I., Agafonova, J., Gerasimenko, N., Averchenkova, A., Mironova, E., Bukashkin, A., Kulikov, K., et al.: Kandinsky 3: Text-to-image synthesis for multifunctional generative framework. In: Empirical Methods in Natural Language Processing (2024)

[6] Avrahami, O., Fried, O., Lischinski, D.: Blended latent diffusion. ACM Transactions on Graphics (2023)

[7] Avrahami, O., Lischinski, D., Fried, O.: Blended diffusion for text-driven editing of natural images. In: IEEE Conference on Computer Vision and Pattern Recognition (2022)

[8] Bianchi, T., Piva, A.: Image forgery localization via block-grained analysis of jpeg artifacts. IEEE Transactions on Information Forensics and Security (2012)

[9] Black Forest Labs: Announcing black forest labs. https://bfl.ai/announcements/24-08-01-bfl (2024)

[10] Blakemore, E.: How photos became a weapon in stalin's great purge. Canal História (2019)

[11] Caron, M., Touvron, H., Misra, I., Jégou, H., Mairal, J., Bojanowski, P., Joulin, A.: Emerging properties in self-supervised vision transformers. In: International Conference on Computer Vision (2021)

[12] de Carvalho, T.J., Riess, C., Angelopoulou, E., Pedrini, H., de Rezende Rocha, A.: Exposing digital image forgeries by illumination color classification. IEEE Transactions on Information Forensics and Security (2013)

[13] Cazenavette, G., Sud, A., Leung, T., Usman, B.: Fakeinversion: Learning to detect images from unseen text-to-image models by inverting stable diffusion. In: IEEE Conference on Computer Vision and Pattern Recognition (2024)

[14] Chen, C.F.R., Fan, Q., Panda, R.: Crossvit: Cross-attention multi-scale vision transformer for image classification. In: International Conference on Computer Vision (2021)

[15] Chen, J., Wu, Y., Luo, S., Xie, E., Paul, S., Luo, P., Zhao, H., Li, Z.: Pixart-δ: Fast and controllable image generation with latent consistency models (2024)

[16] Chen, T., Kornblith, S., Norouzi, M., Hinton, G.: A simple framework for contrastive learning of visual representations. In: International Conference on Machine Learning (2020)

[17] Chen, Y., Yin, W., Luo, A., Yang, J., Wang, J.: Improving the generalization and robustness of computer-generated image detection based on contrastive learning. International Journal of Intelligent Systems (2025)

[18] Chen, Y., Huang, X., Zhang, Q., Li, W., Zhu, M., Yan, Q., Li, S., Chen, H., Hu, H., Yang, J., et al.: Gim: A million-scale benchmark for generative image manipulation detection and localization. In: AAAI Conference on Artificial Intelligence (2025)

[19] Chesney, R., Citron, D.K.: Deep fakes: A looming challenge for privacy, democracy, and national security. California Law Review (2019)

[20] Chu, B., Xu, X., Wang, X., Zhang, Y., You, W., Zhou, L.: Fire: Robust detection of diffusion-generated images via frequency-guided reconstruction error. In: IEEE Conference on Computer Vision and Pattern Recognition (2025)

 https://doi.org/10.52202/085713-1270

[21] Croitoru, F.A., Hondru, V., Ionescu, R.T., Shah, M.: Diffusion models in vision: A survey. IEEE Transactions on Pattern Analysis and Machine Intelligence (2025)

[22] Das, A.S., Pang, G., Bhuyan, M.: Adaptive Deviation Learning for Visual Anomaly Detection with Data Contamination . In: Winter Applications of Computer Vision (2025)

[23] Doloriel, C.T., Cheung, N.M.: Frequency masking for universal deepfake detection. In: IEEE International Conference on Acoustics, Speech, and Signal Processing (2024)

[24] Dong, J., Wang, W., Tan, T.: CASIA image tampering detection evaluation database. In: IEEE China Summit and International Conference on Signal and Information Processing (2013)

[25] Epstein, D.C., Jain, I., Wang, O., Zhang, R.: Online detection of ai-generated images. In: International Conference on Computer Vision (2023)

[26] Esser, P., Kulal, S., Blattmann, A., Entezari, R., Müller, J., Saini, H., Levi, Y., Lorenz, D., Sauer, A., Boesel, F., et al.: Scaling rectified flow transformers for high-resolution image synthesis. In: International Conference on Machine Learning (2024)

[27] FLUX AI: Flux.1 fill [pro]. https://fluxart.ai (2024)

[28] Frank, J., Eisenhofer, T., Schönherr, L., Fischer, A., Kolossa, D., Holz, T.: Leveraging frequency analysis for deep fake image recognition. In: International Conference on Machine Learning (2020)

[29] Fu, K., Fan, D.P., Ji, G.P., Zhao, Q., Shen, J., Zhu, C.: Siamese network for rgb-d salient object detection and beyond. IEEE Transactions on Pattern Analysis and Machine Intelligence (2021)

[30] GPS Media: Dpreview. https://www.dpreview.com/ (1998)

[31] Guan, H., Kozak, M., Robertson, E., Lee, Y., Yates, A.N., Delgado, A., Zhou, D., Kheyrkhah, T., Smith, J., Fiscus, J.: Mfc datasets: Large-scale benchmark datasets for media forensic challenge evaluation. In: Winter Applications of Computer Vision Workshops (2019)

[32] Guillaro, F., Cozzolino, D., Sud, A., Dufour, N., Verdoliva, L.: Trufor: Leveraging all-round clues for trustworthy image forgery detection and localization. In: IEEE Conference on Computer Vision and Pattern Recognition (2023)

[33] Guo, X., Liu, X., Ren, Z., Grosz, S., Masi, I., Liu, X.: Hierarchical fine-grained image forgery detection and localization. In: IEEE Conference on Computer Vision and Pattern Recognition (2023)

[34] Hancock, J.T., Bailenson, J.N.: The social impact of deepfakes. Cyberpsychology, behavior, and social networking (2021)

[35] Hendrycks, D., Basart, S., Mu, N., Kadavath, S., Wang, F., Dorundo, E., Desai, R., Zhu, T., Parajuli, S., Guo, M., et al.: The many faces of robustness: A critical analysis of out-of-distribution generalization. In: International Conference on Computer Vision (2021)

[36] Hong, Y., Zhang, J.: Wildfake: A large-scale challenging dataset for ai-generated images detection. In: AAAI Conference on Artificial Intelligence (2025)

[37] Hsu, Y.f., Chang, S.F.: Detecting image splicing using geometry invariants and camera characteristics consistency. In: IEEE International Conference on Multimedia and Expo (ICME) (2006)

[38] Huang, Y., Huang, J., Liu, Y., Yan, M., Lv, J., Liu, J., Xiong, W., Zhang, H., Cao, L., Chen, S.: Diffusion model-based image editing: A survey. IEEE Transactions on Pattern Analysis and Machine Intelligence (2025)

[39] Huang, Z., Hu, J., Li, X., He, Y., Zhao, X., Peng, B., Wu, B., Huang, X., Cheng, G.: Sida: Social media image deepfake detection, localization and explanation with large multimodal model. In: IEEE Conference on Computer Vision and Pattern Recognition (2025)

[40] Ideogram Inc.: Ideogram. https://ideogram.ai (2023)

[41] Jia, S., Huang, M., Zhou, Z., Ju, Y., Cai, J., Lyu, S.: Autosplice: A text-prompt manipulated image dataset for media forensics. In: IEEE Conference on Computer Vision and Pattern Recognition Workshops (2023)

[42] Khosla, P., Teterwak, P., Wang, C., Sarna, A., Tian, Y., Isola, P., Maschinot, A., Liu, C., Krishnan, D.: Supervised contrastive learning. In: Advances on Neural Information Processing Systems (2020)

[43] Khosla, P., Teterwak, P., Wang, C., Sarna, A., Tian, Y., Isola, P., Maschinot, A., Liu, C., Krishnan, D.: Supervised contrastive learning. Advances on Neural Information Processing Systems (2020)

[44] Kingma, D.P., Ba, J.: Adam: A method for stochastic optimization. In: International Conference on Learning Representations (2015)

[45] Kwon, M.J., Lee, W., Nam, S.H., Son, M., Kim, C.: Safire: Segment any forged image region. In: AAAI Conference on Artificial Intelligence (2025)

[46] Li, S., Ma, W., Guo, J., Xu, S., Li, B., Zhang, X.: Unionformer: Unified-learning transformer with multi-view representation for image manipulation detection and localization. In: IEEE Conference on Computer Vision and Pattern Recognition (2024)

[47] Li, Y., Bian, Y., Ju, X., Zhang, Z., Shan, Y., Zou, Y., Xu, Q.: Brushedit: All-in-one image inpainting and editing. arXiv preprint arXiv:2412.10316 (2024)

[48] Li, Y., Cheng, F., Yu, W., Wang, G., Luo, G., Zhu, Y.: Adaifl: Adaptive image forgery localization via a dynamic and importance-aware transformer network. In: European Conference on Computer Vision (2025)

[49] Liu, H., Wang, Y., Qian, B., Wang, M., Rui, Y.: Structure matters: Tackling the semantic discrepancy in diffusion models for image inpainting. In: IEEE Conference on Computer Vision and Pattern Recognition (2024)

[50] LLC, G.: Open images dataset. https://storage.googleapis.com/openimages/web/index.html (2020)

[51] McInnes, L., Healy, J., Melville, J.: Umap: Uniform manifold approximation and projection for dimension reduction. arXiv preprint arXiv:1802.03426 (2018)

[52] Nichol, A., Dhariwal, P., Ramesh, A., Shyam, P., Mishkin, P., McGrew, B., Sutskever, I., Chen, M.: Glide: Towards photorealistic image generation and editing with text-guided diffusion models (2022)

[53] Novozamsky, A., Mahdian, B., Saic, S.: IMD2020: A large-scale annotated dataset tailored for detecting manipulated images. In: Winter Applications of Computer Vision (2020)

[54] Ojha, U., Li, Y., Lee, Y.J.: Towards universal fake image detectors that generalize across generative models. In: IEEE Conference on Computer Vision and Pattern Recognition (2023)

[55] OpenAI: Dall·e 2. https://openai.com/dall-e-2 (2022)

[56] Oquab, M., Darcet, T., Moutakanni, T., Vo, H., Szafraniec, M., Khalidov, V., Fernandez, P., Haziza, D., Massa, F., El-Nouby, A., et al.: Dinov2: Learning robust visual features without supervision. Transactions on Machine Learning Research (2024)

[57] Park, J., Owens, A.: Community forensics: Using thousands of generators to train fake image detectors. In: IEEE Conference on Computer Vision and Pattern Recognition (2025)

[58] Peng, Z., Wang, W., Dong, L., Hao, Y., Huang, S., Ma, S., Wei, F.: Kosmos-2: Grounding multimodal large language models to the world. In: International Conference on Learning Representations (2024)

[59] Perfect Corp.: Youcam. https://www.perfectcorp.com/consumer/apps/youcam-makeup (2014)

 https://doi.org/10.52202/085713-1270

[60] Phot.AI: Phot.ai. https://www.phot.ai (2023)

[61] von Platen, P., Patil, S., Lozhkov, A., Cuenca, P., Lambert, N., Rasul, K., Davaadorj, M., Nair, D., Paul, S., Berman, W., Xu, Y., Liu, S., Wolf, T.: Diffusers: State-of-the-art diffusion models. https://github.com/huggingface/diffusers (2022)

[62] Podell, D., English, Z., Lacey, K., Blattmann, A., Dockhorn, T., Müller, J., Penna, J., Rombach, R.: Sdxl: Improving latent diffusion models for high-resolution image synthesis. In: International Conference on Learning Representations (2024)

[63] Qu, C., Zhong, Y., Liu, C., Xu, G., Peng, D., Guo, F., Jin, L.: Towards modern image manipulation localization: A large-scale dataset and novel methods. In: IEEE Conference on Computer Vision and Pattern Recognition (2024)

[64] Razzhigaev, A., Shakhmatov, A., Maltseva, A., Arkhipkin, V., Pavlov, I., Ryabov, I., Kuts, A., Panchenko, A., Kuznetsov, A., Dimitrov, D.: Kandinsky: an improved text-to-image synthesis with image prior and latent diffusion. In: Empirical Methods in Natural Language Processing (2023)

[65] Ren, T., Liu, S., Zeng, A., Lin, J., Li, K., Cao, H., Chen, J., Huang, X., Chen, Y., Yan, F., et al.: Grounded sam: Assembling open-world models for diverse visual tasks. arXiv preprint arXiv:2401.14159 (2024)

[66] Ricker, J., Lukovnikov, D., Fischer, A.: Aeroblade: Training-free detection of latent diffusion images using autoencoder reconstruction error. In: IEEE Conference on Computer Vision and Pattern Recognition (2024)

[67] Rodriguez-Ortega, Y., Ballesteros, D.M., Renza, D.: Copy-move forgery detection (cmfd) using deep learning for image and video forensics. Journal of Imaging (2021)

[68] Rombach, R., Blattmann, A., Lorenz, D., Esser, P., Ommer, B.: High-resolution image synthesis with latent diffusion models. In: IEEE Conference on Computer Vision and Pattern Recognition (2022)

[69] Saharia, C., Chan, W., Saxena, S., Li, L., Whang, J., Denton, E.L., Ghasemipour, K., Gontijo Lopes, R., Karagol Ayan, B., Salimans, T., Ho, J., Fleet, D.J., Norouzi, M.: Photorealistic text-to-image diffusion models with deep language understanding. In: Advances on Neural Information Processing Systems (2022)

[70] Sarkar, A., Mai, H., Mahapatra, A., Lazebnik, S., Forsyth, D.A., Bhattad, A.: Shadows don't lie and lines can't bend! generative models don't know projective geometry... for now. In: IEEE Conference on Computer Vision and Pattern Recognition (2024)

[71] Schuhmann, C., Beaumont, R., Vencu, R., Gordon, C., Wightman, R., Cherti, M., Coombes, T., Katta, A., Mullis, C., Wortsman, M., et al.: Laion-5b: An open large-scale dataset for training next generation image-text models. Advances on Neural Information Processing Systems (2022)

[72] Stability AI: Clipdrop. https://clipdrop.co (2020)

[73] Sudre, C.H., Li, W., Vercauteren, T., Ourselin, S., Jorge Cardoso, M.: Generalised dice overlap as a deep learning loss function for highly unbalanced segmentations. In: The International Conference on Medical Image Computing and Computer Assisted Intervention Workshops (2017)

[74] Tan, C., Tao, R., Liu, H., Gu, G., Wu, B., Zhao, Y., Wei, Y.: C2p-clip: Injecting category common prompt in clip to enhance generalization in deepfake detection. In: AAAI Conference on Artificial Intelligence (2025)

[75] Torralba, A., Efros, A.A.: Unbiased look at dataset bias. In: IEEE Conference on Computer Vision and Pattern Recognition (2011)

[76] Tsai, Y.H.H., Bai, S., Liang, P.P., Kolter, J.Z., Morency, L.P., Salakhutdinov, R.: Multimodal transformer for unaligned multimodal language sequences. In: The Annual Meeting of the Association for Computational Linguistics (2019)

[77] Vaccari, C., Chadwick, A.: Deepfakes and disinformation: Exploring the impact of synthetic political video on deception, uncertainty, and trust in news. Social Media+ Society (2020)

[78] Wang, J., Wu, Z., Chen, J., Han, X., Shrivastava, A., Lim, S.N., Jiang, Y.G.: Objectformer for image manipulation detection and localization. In: IEEE Conference on Computer Vision and Pattern Recognition (2022)

[79] Wang, P., Shen, X., Lin, Z., Cohen, S., Price, B., Yuille, A.L.: Towards unified depth and semantic prediction from a single image. In: IEEE Conference on Computer Vision and Pattern Recognition (2015)

[80] Wang, S.Y., Wang, O., Zhang, R., Owens, A., Efros, A.A.: Cnn-generated images are surprisingly easy to spot... for now. In: IEEE Conference on Computer Vision and Pattern Recognition (2020)

[81] Wang, S., Saharia, C., Montgomery, C., Pont-Tuset, J., Noy, S., Pellegrini, S., Onoe, Y., Laszlo, S., Fleet, D.J., Soricut, R., Baldridge, J., Norouzi, M., Anderson, P., Chan, W.: Imagen editor and editbench: Advancing and evaluating text-guided image inpainting. arXiv preprint arXiv:2212.06909 (2023)

[82] Wang, Y., Huang, Z., Hong, X.: Opensdi: Spotting diffusion-generated images in the open world. In: IEEE Conference on Computer Vision and Pattern Recognition (2025)

[83] Wang, Z., Bao, J., Zhou, W., Wang, W., Hu, H., Chen, H., Li, H.: Dire for diffusion-generated image detection. In: International Conference on Computer Vision (2023)

[84] Wen, B., Zhu, Y., Subramanian, R., Ng, T.T., Shen, X., Winkler, S.: COVERAGE — A novel database for copy-move forgery detection. In: IEEE International Conference on Image Processing (2016)

[85] Wen, S., Ye, J., Feng, P., Kang, H., Wen, Z., Chen, Y., Wu, J., Wu, W., He, C., Li, W.: Spot the fake: Large multimodal model-based synthetic image detection with artifact explanation. arXiv preprint arXiv:2503.14905 (2025)

[86] Xu, Z., Zhang, X., Li, R., Tang, Z., Huang, Q., Zhang, J.: Fakeshield: Explainable image forgery detection and localization via multi-modal large language models. In: International Conference on Learning Representations (2025)

[87] Yan, S., Li, O., Cai, J., Hao, Y., Jiang, X., Hu, Y., Xie, W.: A sanity check for ai-generated image detection. In: International Conference on Learning Representations (2025)

[88] Yang, L., Kang, B., Huang, Z., Zhao, Z., Xu, X., Feng, J., Zhao, H.: Depth anything v2. In: Advances on Neural Information Processing Systems (2024)

[89] Yu, T., Feng, R., Feng, R., Liu, J., Jin, X., Zeng, W., Chen, Z.: Inpaint anything: Segment anything meets image inpainting. arXiv preprint arXiv:2304.06790 (2023)

[90] Zavrtanik, V., Kristan, M., Skocaj, D.: Draem - a discriminatively trained reconstruction embedding for surface anomaly detection. In: International Conference on Computer Vision (2021)

[91] Zeng, Z., Liu, H., Peng, D., Jin, L., Watanabe, H.: Time step generating: A universal synthesized deepfake image detector. arXiv preprint arXiv:2411.11016 (2024)

[92] Zhang, Z., Chang, M.C., Li, X.: Training-free image manipulation localization using diffusion models. In: AAAI Conference on Artificial Intelligence (2025)

[93] Zhu, S., Brazil, G., Liu, X.: The edge of depth: Explicit constraints between segmentation and depth. In: IEEE Conference on Computer Vision and Pattern Recognition (2020)

[94] Zhu, X., Ma, X., Su, L., Jiang, Z., Du, B., Wang, X., Lei, Z., Feng, W., Pun, C.M., Zhou, J.: Mesoscopic insights: Orchestrating multi-scale & hybrid architecture for image manipulation localization. In: AAAI Conference on Artificial Intelligence (2025)

 https://doi.org/10.52202/085713-1270

NeurIPS Paper Checklist

1. **Claims**

   Question: Do the main claims made in the abstract and introduction accurately reflect the paper's contributions and scope?

   Answer: [Yes] .

   Justification: the abstract outlines both the benchmark and the method that are presented in detail in the rest of the paper.

   Guidelines:

   - The answer NA means that the abstract and introduction do not include the claims made in the paper.
   - The abstract and/or introduction should clearly state the claims made, including the contributions made in the paper and important assumptions and limitations. A No or NA answer to this question will not be perceived well by the reviewers.
   - The claims made should match theoretical and experimental results, and reflect how much the results can be expected to generalize to other settings.
   - It is fine to include aspirational goals as motivation as long as it is clear that these goals are not attained by the paper.

2. **Limitations**

   Question: Does the paper discuss the limitations of the work performed by the authors?

   Answer: [Yes] .

   Justification: limitations of the work are mentioned in the conclusion of the paper and discussed in the appendix.

   Guidelines:

   - The answer NA means that the paper has no limitation while the answer No means that the paper has limitations, but those are not discussed in the paper.
   - The authors are encouraged to create a separate "Limitations" section in their paper.
   - The paper should point out any strong assumptions and how robust the results are to violations of these assumptions (e.g., independence assumptions, noiseless settings, model well-specification, asymptotic approximations only holding locally). The authors should reflect on how these assumptions might be violated in practice and what the implications would be.
   - The authors should reflect on the scope of the claims made, e.g., if the approach was only tested on a few datasets or with a few runs. In general, empirical results often depend on implicit assumptions, which should be articulated.
   - The authors should reflect on the factors that influence the performance of the approach. For example, a facial recognition algorithm may perform poorly when image resolution is low or images are taken in low lighting. Or a speech-to-text system might not be used reliably to provide closed captions for online lectures because it fails to handle technical jargon.
   - The authors should discuss the computational efficiency of the proposed algorithms and how they scale with dataset size.
   - If applicable, the authors should discuss possible limitations of their approach to address problems of privacy and fairness.
   - While the authors might fear that complete honesty about limitations might be used by reviewers as grounds for rejection, a worse outcome might be that reviewers discover limitations that aren't acknowledged in the paper. The authors should use their best judgment and recognize that individual actions in favor of transparency play an important role in developing norms that preserve the integrity of the community. Reviewers will be specifically instructed to not penalize honesty concerning limitations.

3. **Theory assumptions and proofs**

   Question: For each theoretical result, does the paper provide the full set of assumptions and a complete (and correct) proof?

   Answer: [NA] .

   Justification: the paper does not include theoretical results.

Guidelines:

- The answer NA means that the paper does not include theoretical results.
- All the theorems, formulas, and proofs in the paper should be numbered and cross-referenced.
- All assumptions should be clearly stated or referenced in the statement of any theorems.
- The proofs can either appear in the main paper or the supplemental material, but if they appear in the supplemental material, the authors are encouraged to provide a short proof sketch to provide intuition.
- Inversely, any informal proof provided in the core of the paper should be complemented by formal proofs provided in appendix or supplemental material.
- Theorems and Lemmas that the proof relies upon should be properly referenced.

4. **Experimental result reproducibility**

   Question: Does the paper fully disclose all the information needed to reproduce the main experimental results of the paper to the extent that it affects the main claims and/or conclusions of the paper (regardless of whether the code and data are provided or not)?

   Answer: [Yes] .

   Justification: all the implementation details of the method are specified, and random seeds are fixed across all experiments. Moreover, the code will be released upon eventual acceptance with both train and evaluation scripts, along with the model's checkpoint.

   Guidelines:

   - The answer NA means that the paper does not include experiments.
   - If the paper includes experiments, a No answer to this question will not be perceived well by the reviewers: Making the paper reproducible is important, regardless of whether the code and data are provided or not.
   - If the contribution is a dataset and/or model, the authors should describe the steps taken to make their results reproducible or verifiable.
   - Depending on the contribution, reproducibility can be accomplished in various ways. For example, if the contribution is a novel architecture, describing the architecture fully might suffice, or if the contribution is a specific model and empirical evaluation, it may be necessary to either make it possible for others to replicate the model with the same dataset, or provide access to the model. In general. releasing code and data is often one good way to accomplish this, but reproducibility can also be provided via detailed instructions for how to replicate the results, access to a hosted model (e.g., in the case of a large language model), releasing of a model checkpoint, or other means that are appropriate to the research performed.
   - While NeurIPS does not require releasing code, the conference does require all submissions to provide some reasonable avenue for reproducibility, which may depend on the nature of the contribution. For example
     (a) If the contribution is primarily a new algorithm, the paper should make it clear how to reproduce that algorithm.
     (b) If the contribution is primarily a new model architecture, the paper should describe the architecture clearly and fully.
     (c) If the contribution is a new model (e.g., a large language model), then there should either be a way to access this model for reproducing the results or a way to reproduce the model (e.g., with an open-source dataset or instructions for how to construct the dataset).
     (d) We recognize that reproducibility may be tricky in some cases, in which case authors are welcome to describe the particular way they provide for reproducibility. In the case of closed-source models, it may be that access to the model is limited in some way (e.g., to registered users), but it should be possible for other researchers to have some path to reproducing or verifying the results.

5. **Open access to data and code**

   Question: Does the paper provide open access to the data and code, with sufficient instructions to faithfully reproduce the main experimental results, as described in supplemental material?

   Answer: [Yes] .

https://doi.org/10.52202/085713-1270

Justification: the code for both method and data generation will be released upon eventual acceptance. Moreover, most of the generated data will be released as well. Part of the generated data cannot be released due to licensing issues; however, since the starting data is open source and the data generation code will be released, it will be possible to generate the same data as well.

Guidelines:

- The answer NA means that paper does not include experiments requiring code.
- Please see the NeurIPS code and data submission guidelines (https://nips.cc/public/guides/CodeSubmissionPolicy) for more details.
- While we encourage the release of code and data, we understand that this might not be possible, so "No" is an acceptable answer. Papers cannot be rejected simply for not including code, unless this is central to the contribution (e.g., for a new open-source benchmark).
- The instructions should contain the exact command and environment needed to run to reproduce the results. See the NeurIPS code and data submission guidelines (https://nips.cc/public/guides/CodeSubmissionPolicy) for more details.
- The authors should provide instructions on data access and preparation, including how to access the raw data, preprocessed data, intermediate data, and generated data, etc.
- The authors should provide scripts to reproduce all experimental results for the new proposed method and baselines. If only a subset of experiments are reproducible, they should state which ones are omitted from the script and why.
- At submission time, to preserve anonymity, the authors should release anonymized versions (if applicable).
- Providing as much information as possible in supplemental material (appended to the paper) is recommended, but including URLs to data and code is permitted.

6. **Experimental setting/details**

   Question: Does the paper specify all the training and test details (e.g., data splits, hyperparameters, how they were chosen, type of optimizer, etc.) necessary to understand the results?

   Answer: [Yes] .

   Justification: experimental details are mentioned both in the main paper and its appendix. Moreover, the code will contain the final train and test scripts employed for the main tables experiments.

   Guidelines:

   - The answer NA means that the paper does not include experiments.
   - The experimental setting should be presented in the core of the paper to a level of detail that is necessary to appreciate the results and make sense of them.
   - The full details can be provided either with the code, in appendix, or as supplemental material.

7. **Experiment statistical significance**

   Question: Does the paper report error bars suitably and correctly defined or other appropriate information about the statistical significance of the experiments?

   Answer: [No] .

   Justification: not all experiments have been run multiple times since it would be too time and resource-consuming. However, the inference is deterministic and random seeds have been fixed to ensure stability in the experiments.

   Guidelines:

   - The answer NA means that the paper does not include experiments.
   - The authors should answer "Yes" if the results are accompanied by error bars, confidence intervals, or statistical significance tests, at least for the experiments that support the main claims of the paper.
   - The factors of variability that the error bars are capturing should be clearly stated (for example, train/test split, initialization, random drawing of some parameter, or overall run with given experimental conditions).

- The method for calculating the error bars should be explained (closed form formula, call to a library function, bootstrap, etc.)
- The assumptions made should be given (e.g., Normally distributed errors).
- It should be clear whether the error bar is the standard deviation or the standard error of the mean.
- It is OK to report 1-sigma error bars, but one should state it. The authors should preferably report a 2-sigma error bar than state that they have a 96% CI, if the hypothesis of Normality of errors is not verified.
- For asymmetric distributions, the authors should be careful not to show in tables or figures symmetric error bars that would yield results that are out of range (e.g. negative error rates).
- If error bars are reported in tables or plots, The authors should explain in the text how they were calculated and reference the corresponding figures or tables in the text.

8. **Experiments compute resources**

   Question: For each experiment, does the paper provide sufficient information on the computer resources (type of compute workers, memory, time of execution) needed to reproduce the experiments?

   Answer: [Yes] .

   Justification: details on the machine employed are included in the training details.

   Guidelines:

   - The answer NA means that the paper does not include experiments.
   - The paper should indicate the type of compute workers CPU or GPU, internal cluster, or cloud provider, including relevant memory and storage.
   - The paper should provide the amount of compute required for each of the individual experimental runs as well as estimate the total compute.
   - The paper should disclose whether the full research project required more compute than the experiments reported in the paper (e.g., preliminary or failed experiments that didn't make it into the paper).

9. **Code of ethics**

   Question: Does the research conducted in the paper conform, in every respect, with the NeurIPS Code of Ethics https://neurips.cc/public/EthicsGuidelines?

   Answer: [Yes] .

   Justification: we reviewed the NeurIPS Code of Ethics.

   Guidelines:

   - The answer NA means that the authors have not reviewed the NeurIPS Code of Ethics.
   - If the authors answer No, they should explain the special circumstances that require a deviation from the Code of Ethics.
   - The authors should make sure to preserve anonymity (e.g., if there is a special consideration due to laws or regulations in their jurisdiction).

10. **Broader impacts**

    Question: Does the paper discuss both potential positive societal impacts and negative societal impacts of the work performed?

    Answer: [Yes] .

    Justification: these impacts are mentioned in the abstract and introduction of the paper, and also addressed in the appendix. The main purpose of the paper is to counteract a malicious use of artificial intelligence, *i.e.*, detection of manipulation on visual data.

    Guidelines:

    - The answer NA means that there is no societal impact of the work performed.
    - If the authors answer NA or No, they should explain why their work has no societal impact or why the paper does not address societal impact.
    - Examples of negative societal impacts include potential malicious or unintended uses (e.g., disinformation, generating fake profiles, surveillance), fairness considerations (e.g., deployment of technologies that could make decisions that unfairly impact specific groups), privacy considerations, and security considerations.

https://doi.org/10.52202/085713-1270

- The conference expects that many papers will be foundational research and not tied to particular applications, let alone deployments. However, if there is a direct path to any negative applications, the authors should point it out. For example, it is legitimate to point out that an improvement in the quality of generative models could be used to generate deepfakes for disinformation. On the other hand, it is not needed to point out that a generic algorithm for optimizing neural networks could enable people to train models that generate Deepfakes faster.
- The authors should consider possible harms that could arise when the technology is being used as intended and functioning correctly, harms that could arise when the technology is being used as intended but gives incorrect results, and harms following from (intentional or unintentional) misuse of the technology.
- If there are negative societal impacts, the authors could also discuss possible mitigation strategies (e.g., gated release of models, providing defenses in addition to attacks, mechanisms for monitoring misuse, mechanisms to monitor how a system learns from feedback over time, improving the efficiency and accessibility of ML).

11. **Safeguards**

    Question: Does the paper describe safeguards that have been put in place for responsible release of data or models that have a high risk for misuse (e.g., pretrained language models, image generators, or scraped datasets)?

    Answer: [Yes] .

    Justification: these implications are discussed and addressed in the appendix.

    Guidelines:

    - The answer NA means that the paper poses no such risks.
    - Released models that have a high risk for misuse or dual-use should be released with necessary safeguards to allow for controlled use of the model, for example by requiring that users adhere to usage guidelines or restrictions to access the model or implementing safety filters.
    - Datasets that have been scraped from the Internet could pose safety risks. The authors should describe how they avoided releasing unsafe images.
    - We recognize that providing effective safeguards is challenging, and many papers do not require this, but we encourage authors to take this into account and make a best faith effort.

12. **Licenses for existing assets**

    Question: Are the creators or original owners of assets (e.g., code, data, models), used in the paper, properly credited and are the license and terms of use explicitly mentioned and properly respected?

    Answer: [Yes] .

    Justification: the creators and original owners of assets are properly credited, and license and terms of use are explicitly mentioned in the supplemental material and properly respected.

    Guidelines:

    - The answer NA means that the paper does not use existing assets.
    - The authors should cite the original paper that produced the code package or dataset.
    - The authors should state which version of the asset is used and, if possible, include a URL.
    - The name of the license (e.g., CC-BY 4.0) should be included for each asset.
    - For scraped data from a particular source (e.g., website), the copyright and terms of service of that source should be provided.
    - If assets are released, the license, copyright information, and terms of use in the package should be provided. For popular datasets, `paperswithcode.com/datasets` has curated licenses for some datasets. Their licensing guide can help determine the license of a dataset.
    - For existing datasets that are re-packaged, both the original license and the license of the derived asset (if it has changed) should be provided.
    - If this information is not available online, the authors are encouraged to reach out to the asset's creators.

13. **New assets**

    Question: Are new assets introduced in the paper well documented and is the documentation provided alongside the assets?

    Answer: [Yes] .

    Justification: the code released upon eventual acceptance will provide proper documentation with instructions to run both train and evaluation scripts, along with the final model's checkpoint.

    Guidelines:

    - The answer NA means that the paper does not release new assets.
    - Researchers should communicate the details of the dataset/code/model as part of their submissions via structured templates. This includes details about training, license, limitations, etc.
    - The paper should discuss whether and how consent was obtained from people whose asset is used.
    - At submission time, remember to anonymize your assets (if applicable). You can either create an anonymized URL or include an anonymized zip file.

14. **Crowdsourcing and research with human subjects**

    Question: For crowdsourcing experiments and research with human subjects, does the paper include the full text of instructions given to participants and screenshots, if applicable, as well as details about compensation (if any)?

    Answer: [NA] .

    Justification: the paper does not involve crowdsourcing nor research with human subjects.

    Guidelines:

    - The answer NA means that the paper does not involve crowdsourcing nor research with human subjects.
    - Including this information in the supplemental material is fine, but if the main contribution of the paper involves human subjects, then as much detail as possible should be included in the main paper.
    - According to the NeurIPS Code of Ethics, workers involved in data collection, curation, or other labor should be paid at least the minimum wage in the country of the data collector.

15. **Institutional review board (IRB) approvals or equivalent for research with human subjects**

    Question: Does the paper describe potential risks incurred by study participants, whether such risks were disclosed to the subjects, and whether Institutional Review Board (IRB) approvals (or an equivalent approval/review based on the requirements of your country or institution) were obtained?

    Answer: [NA] .

    Justification: the paper does not involve crowdsourcing nor research with human subjects.

    Guidelines:

    - The answer NA means that the paper does not involve crowdsourcing nor research with human subjects.
    - Depending on the country in which research is conducted, IRB approval (or equivalent) may be required for any human subjects research. If you obtained IRB approval, you should clearly state this in the paper.
    - We recognize that the procedures for this may vary significantly between institutions and locations, and we expect authors to adhere to the NeurIPS Code of Ethics and the guidelines for their institution.
    - For initial submissions, do not include any information that would break anonymity (if applicable), such as the institution conducting the review.

16. **Declaration of LLM usage**

    Question: Does the paper describe the usage of LLMs if it is an important, original, or non-standard component of the core methods in this research? Note that if the LLM is used

https://doi.org/10.52202/085713-1270

only for writing, editing, or formatting purposes and does not impact the core methodology, scientific rigorousness, or originality of the research, declaration is not required.

Answer: [NA] .

Justification: LLMs have been exclusively employed as a syntax checker integrated in the text editor.

Guidelines:

- The answer NA means that the core method development in this research does not involve LLMs as any important, original, or non-standard components.
- Please refer to our LLM policy (https://neurips.cc/Conferences/2025/LLM) for what should or should not be described.

Appendix

In this document, we propose complementary information to the main paper. First, we list all assets used in Appendix A. Then, we report details for the reimplementation in Appendix B, including also details on the construction of BBC-PAIR. We provide extensive additional analysis, results, and ablations in Appendix C, while we propose final remarks and limitations in Section D.

A Assets

A.1 Methods

For all the competitors [33, 32, 63, 48, 94, 45, 39], we employed their official implementations. In particular:

- Hifi-Net: https://github.com/CHELSEA234/HiFi_IFDL released under MIT license;
- TruFor: https://github.com/grip-unina/TruFor released under MIT license;
- MIML: https://github.com/qcf-568/MIML release under a custom licensing scheme;
- AdaIFL: https://github.com/LMIAPC/AdaIFL released under MIT license;
- Mesorch: https://github.com/scu-zjz/Mesorch released under MIT license;
- SAFIRE: https://github.com/mjkwon2021/SAFIRE released under CC BY-NC 4.0 license;
- SIDA: https://github.com/hzlsaber/SIDA released under a custom licensing scheme.

We thank the respective authors for making their code and pre-trained model weights publicly available, and for promptly and helpfully replying to our inquiries.

A.2 Datasets

For the creation of BBC-PAIR, we gathered data from the following datasets:

- OpenImages-v7: https://storage.googleapis.com/openimages/web/index.html, released under Apache 2.0 license;
- CocoGlide: https://github.com/grip-unina/TruFor released under MIT license;
- SID-Set: https://huggingface.co/datasets/saberzl/SID_Set released under Creative Commons Attribution 4.0 International License;
- SafireMS-Expert: https://www.kaggle.com/datasets/qsii24/safire-safirems-expert-multi-source-dataset released under CC BY-NC 4.0 license.

Moreover, since SafireMS-Expert provided only tampered images, in order to be able to assess the detection performance between genuine and tampered images, we augmented the dataset with genuine images. These images come from DPREVIEW [30], the same source used to create the tampered ones, creating SafireMS-Expert++. We introduced a number of images equal to the number of tampered images present in SafireMS-Expert, obtaining a balanced set.

A.3 Inpainters

To create BBC-PAIR, we employed open-source inpainters [68, 26, 62, 5, 64, 9], LoRA adaptations and commercial inpainters [72, 55, 1, 27, 40, 4, 60, 59]. In particular, for open-source inpainters, we leveraged:

- Stable Diffusion 1.4: https://huggingface.co/CompVis/stable-diffusion-v1-4 released under CreativeML OpenRAIL-M license;
- Stable Diffusion 1.5: https://huggingface.co/stable-diffusion-v1-5/stable-diffusion-v1-5 released under CreativeML OpenRAIL-M license;
- Stable Diffusion 2.1: https://huggingface.co/stabilityai/stable-diffusion-2-1 released under CreativeML OpenRAIL-M license;
- Stable Diffusion 3: https://github.com/replicate/cog-stable-diffusion-3 released under Apache 2.0 license;
- Stable Diffusion 3.5: https://github.com/Stability-AI/sd3.5 released under MIT license;

https://doi.org/10.52202/085713-1270

- Stable Diffusion XL: https://huggingface.co/docs/diffusers/en/using-diffusers/sdxl released under MIT license;
- Kandinsky 2.2: https://github.com/ai-forever/Kandinsky-2 released under Apache 2.0 license;
- Kandinsky 3.1: https://github.com/ai-forever/Kandinsky-3 released under Apache 2.0 license;
- FLUX.1-schnell: https://github.com/black-forest-labs/flux released under Apache 2.0 license;
- FLUX.1-dev: https://github.com/black-forest-labs/flux released under non-commercial license;

Then, for LoRA adaptations, we employed:

- dAIversity Detailer 1.5: https://www.shakker.ai/fil/modelinfo/3ecae938ab8c4aa4a65f6fc104aaad5f;
- dAIversity SD3.5-Large-Photorealistic-LoRA: https://huggingface.co/prithivMLmods/SD3.5-Large-Photorealistic-LoRA;
- Flux-Detailer-LoRA: https://huggingface.co/gokaygokay/Flux-Detailer-LoRA;
- Dreamshaper SDXL-1-0: https://huggingface.co/Lykon/dreamshaper-xl-1-0;
- Juggernaut-XL-v6: https://huggingface.co/RunDiffusion/Juggernaut-XL-v6;
- Perfection 1.5: https://civitai.com/models/411088?modelVersionId=486099
- Perfection Flux: https://civitai.com/models/411088?modelVersionId=931225
- flux-RealismLora: https://huggingface.co/XLabs-AI/flux-RealismLora;
- ReaPhoLoRA 1.5: https://civitai.com/models/59980/realistic-photography
- Yamer's Realsim-v2 XL: https://tensor.art/models/687689251510406883;

Lastly, for commercial inpainters, we relied on:

- ClipDrop: https://clipdrop.co/;
- Dall-E 2: https://openai.com/dall-e;
- Adobe Firefly: https://firefly.adobe.com/;
- FLUX.1 Fill [pro]: https://flux-ml.org/;
- Ideogram: https://ideogram.ai/;
- LightX: https://www.lightxapp.com/;
- Phot.AI: https://www.phot.ai/;
- YouCam: https://www.perfectcorp.com/consumer/apps/ymk.

Each commercial inpainter has its own Terms of Service specified on their website.

B Details for reimplementation

B.1 Construction of BBC-PAIR

Here, we provide detailed information on BBC-PAIR construction. The dataset generation process can be considered as two distinct tasks. The first task involves processing a predetermined cache of base images. These images can originate from any source. The second task involves taking the pre-processed base images and generating an inpainted counterpart for each image per inpainting model.

Dataset pre-processing To begin, each image is checked for correct orientation, as inpainting models typically struggle with images that are not naturally oriented. This is achieved using the open-source library https://github.com/ternaus/check_orientation. Subsequently, each image is processed using Kosmos-2 [58], a model that extracts a wide range of information. For our purposes, we use the image descriptions and annotations provided by Kosmos-2. These annotations include the identification and localisation of objects within the image. Each object identified by Kosmos-2 is then evaluated as a candidate for inclusion in the dataset. The following steps are repeated for each such object:

1. **Segmentation**: the SAM [65] model is used to generate a segmentation mask for each object. It is prompted by Kosmos-2 using the object's location and description;

2. **Size filtering**: the area of the mask is calculated as a percentage of the image area. Objects with masks that are too small or too large are rejected. Specifically, any mask covering more than 83% or less than 0.23% of the image area is discarded. This filtering ensures that inpainted objects are neither minuscule nor encompass the entire image, a common issue with overgeneralised object descriptions from Kosmos-2;
3. **Mask cohesion**: once a mask of acceptable size is found, it is analysed for the number of disconnected components. This serves as a proxy for assessing the cohesiveness of the masked region. If a mask contains too many disconnected components, a dilation operation is applied—up to five times—until the number of components is reduced to fewer than eight. Every mask undergoes at least one dilation to improve cohesiveness for inpainting. If a mask passes all criteria, the following metadata is recorded:
    - Mask number;
    - Original mask;
    - Edited mask;
    - Masked object;
    - Masked area percentage;
    - Mask centroid coordinates.

In addition to object-based masks, a random mask is generated for each image; this is always the last mask generated. This is achieved by randomly selecting eight points and connecting them to form a polygon. The distribution of random mask areas across the dataset is matched to that of the object masks. Each image thus yields at least one random mask and up to ten object-based masks. This step also generates a master JSON file containing metadata for the entire dataset, which is required for the next phase.

Dataset inpainting The second phase of the process involves generating inpainted versions of the base images using one or more inpainting models listed in Appendix A.3. This step can be computationally expensive and is therefore designed to be easily distributed across multiple GPUs and compute nodes. Each inpainting job receives the master JSON file and a subset of the dataset to process. For each image, the model generates a new version using the image's full description and the associated mask, as specified in the JSON.

Due to computational constraints, only the first and last masks for each image are used during inpainting. This ensures that the random mask (always the last) is consistently processed, while the remaining object masks are retained for potential future use.

All inpainting models used are open source, run locally, and rely on the image's full description rather than object-specific text. Empirically, using the full image description yields better inpainting results.

To accommodate different model requirements, images are resized before processing. For models released prior to Stable Diffusion XL (SDXL), images are resized such that the longest edge is 512 pixels. Models released after SDXL use a resized length of 1024 pixels. This resizing enhances the inpainting performance of each model while maintaining consistency. Although inpainting at scale may introduce visual artefacts, the extensive size of the dataset is expected to statistically offset these anomalies.

Once all nodes complete processing, the inpainted images are incorporated into the master JSON file, and all data is aggregated.

B.2 Additional training details

To implement our Multi-modal Encoder, we employ DINO-v2 ViT-B/14 [56] pre-trained on a large, curated and diverse dataset of 142 million images, comprising ImageNet-22k and Depth Anything V2 ViT-B/14 [88], pre-trained on a large mixed dataset comprising millions of real-world (*e.g.*, NYU Depth V2, KITTI, MegaDepth) and synthetic (*e.g.*, BlendedMVS, Virtual KITTI) depth images, enhanced with self-supervised learning on unlabeled web-scale data. The proposed Fusion Block employs bidirectional cross-attention between Semantic and Geometry features. Since the two embedding spaces yield features with different magnitudes, the feature embeddings are layer-normalised before being processed by the Multi-Head Attention heads to avoid overpowering one modality. The features are then processed via two Multi-Head cross-attention layers, with 8 heads

 https://doi.org/10.52202/085713-1270

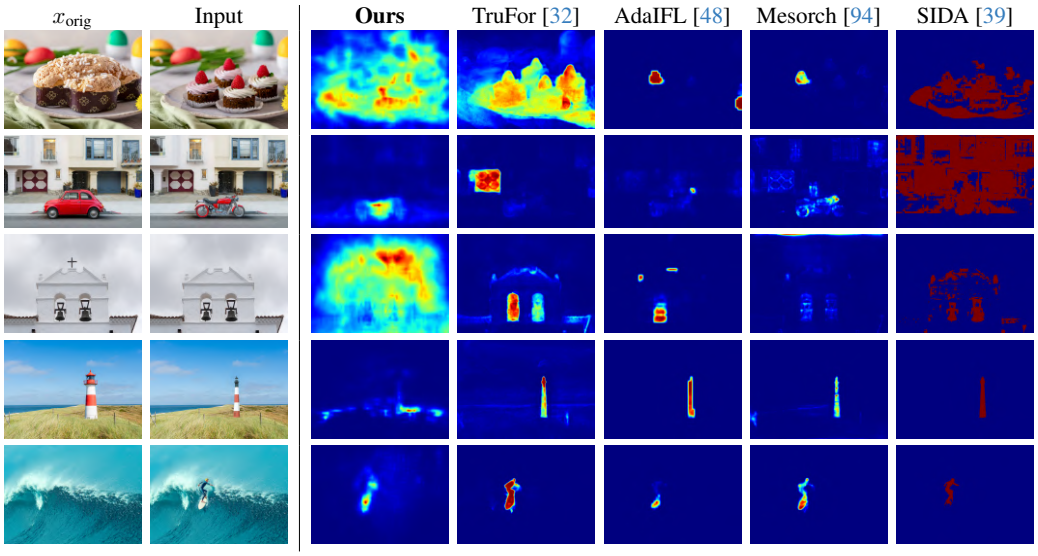


Figure 6: **Qualitative results on tampered in-the-wild images.** Note that SIDA produces a binary output.

each and residual connections, where each modality attends to the other. The mixed features are projected through a single-layer GELU-activated MLP and lastly layer-normalised.

Machine configuration Experiments were conducted on a high-performance computing server equipped with four NVIDIA A100 GPUs (80 GB each, PCIe) and a 96-core CPU, with a total of 866 GB of RAM. The system ran with NVIDIA Driver version 550.144.03 and CUDA Driver version 12.4.

C Additional analysis

C.1 In-the-wild test

We report in Fig. 6 some qualitative samples on in-the-wild tampered images. To obtain these images, we hired a graphic designer with knowledge of inpainting technologies and asked them to download some images from the internet, and modify them with any tool of their choice, as long as it is generative inpainting. By doing so, we obtained 5 pairs of original/tampered images with human-in-the-loop tampering. Please note that we do not have ground truth tampering masks for this task, since many tools do not support saving them. We report original and tampered images, along with the probabilistic prediction localisation maps, in Figure 6. We notice once again how competitors tend to perform well in the presence of a strong semantic tampering (e.g., row 3 and row 4), while failing in the presence of less semantically biased tampering (e.g., row 1, row 2, and row 3). Conversely, RADAR produces a reasonable output in the presence of diverse manipulations, hence being more robust for in-the-wild deployment.

C.2 Impact of the mask size

We propose an additional analysis on the impact of the mask size. We divide the available masks in BBC-PAIR into three sets – "small", "medium", "large" – by ranking them by number of occupied pixels and selecting the corresponding subset. We then evaluate RADAR on the three subsets, reporting results in Table 3. The results show that the detection performance is stable across all sizes. Regarding the localisation performance, on average, we perform better on small masks on BBC-PAIR-ID, while we perform better on large masks on BBC-PAIR-LoRA and BBC-PAIR-OOD. Since there is no clear trend across the three splits, we ascribe these differences to the nature of the specific tamperings rather than their sizes.

https://doi.org/10.52202/085713-1270

Table 3: **Impact of mask size at inference time.**

Setup	ID				LoRA				OOD			
	AUC↑	Acc↑	F1↑	IoU↑	AUC↑	Acc↑	F1↑	IoU↑	AUC↑	Acc↑	F1↑	IoU↑
Small masks	0.951	0.954	0.830	0.704	0.901	0.773	0.720	0.533	0.804	0.712	0.684	0.416
Mid masks	0.951	0.953	0.788	0.665	0.902	0.772	0.599	0.427	0.804	0.706	0.564	0.378
Large masks	0.950	0.954	0.828	0.551	0.902	0.773	0.864	0.539	0.805	0.709	0.834	0.456
All masks	0.945	0.931	0.832	0.600	0.901	0.773	0.810	0.521	0.805	0.709	0.785	0.450

Table 4: **RADAR's performance in low-resource environments.**

Regions	AUC↑	Acc↑	F1↑	IoU↑
All	0.932	0.821	0.802	0.545
Single region	0.930	**0.829**	0.795	0.540
Multiple region	**0.960**	0.712	**0.898**	**0.622**

C.3 Impact of the number of forgeries

Since the Safire-MS Expert subset from MIBench-OOD specifically includes multi-source forgeries, we analysed RADAR's performance on Single Region forgeries (a single connected component in the ground truth) and Multiple Regions (more than one connected component in the ground truth), in Tab. 4. We observe that RADAR's performance remains competitive in both the presence of single regions and multiple regions inpainted. We hypothesise that this is due to the patch-level features separation promoted by our contrastive formulation.

C.4 Performance on non-inpainting datasets

Although RADAR is designed for inpainting tampering only, and trained on inpainting data, we tested its performance on datasets including non-inpainting modifications, namely COVERAGE [84], CASIA-v2 [24], IMD2020 [53], CMFD [67], AutoSplice [41], and DSO [12]. We report results in Table 5. Our performance in localisation is not impacted, in which we achieve even higher F1 than in BBC-PAIR. This is due to the less refined copy-paste operations in these datasets, which, compared to inpainting ones, do not allow for a smooth blending of inserted elements, easing localisation. Importantly, this proves our point about building a dataset specifically focused on inpainting-based modifications. However, we also report lower detection performance. We believe this is due to the lack of distinction between genuine, affected and tampered pixels in non-inpainting modifications, causing outliers in detection. However, since the performance in localisation is satisfactory, a calibration of the detection score could suffice to improve the results.

Interestingly, baselines may report higher accuracies in splicing-based datasets, such as TruFor (*e.g.* AUC/accuracy on COVERAGE 0.770/0.680 in [32]), while falling short on inpainting-based benchmarks such as BBC-PAIR (see Tables 1). We attribute this to the different features important for detection, further motivating our choice to develop an inpainting-specific method for IFDL.

C.5 Additional ablation studies

Detection mechanism ablation We report in Tab. 6 the results obtained by adding an additional classification head to our framework, trained with a binary cross-entropy with image-level labels. This is inspired by alternative frameworks employing similar methodologies [32]. We yield better detection results at the expense of worse localisation results. We observe then a trade-off between the detection and localisation performance in RADAR: in principle, one could train the framework either with a dedicated classifier or not, based on the performance that needs to be prioritised.

Training with random and semantic masks During training of RADAR, we use both semantic masks generated by Grounded SAM and random ones, as we describe in Section 3.1 of the main paper. We report in Tab. 7 the results of training RADAR either with semantic mask-only, random mask-only and mixing both random and semantic masks. We observe how the use of random masks, either

https://doi.org/10.52202/085713-1270

Table 5: **Performance of RADAR on non-inpainting datasets.**

Dataset	AUC↑	Acc↑	F1↑	IoU↑
COVERAGE	0.523	0.535	0.879	0.448
CASIA-v2	0.505	0.505	0.903	0.452
IMD2020	0.597	0.540	0.899	0.454
CMFD	0.517	0.512	0.944	0.474
AutoSplice	0.845	0.743	0.747	0.501
DSO	0.487	0.505	0.854	0.427

Table 6: **Ablation on the use of a dedicated classification head.**

Setup	**ID**				**LoRA**				**OOD**			
	AUC↑	Acc↑	F1↑	IoU↑	AUC↑	Acc↑	F1↑	IoU↑	AUC↑	Acc↑	F1↑	IoU↑
Dedicated `cls` head	**0.957**	**0.898**	0.785	**0.547**	**0.810**	**0.681**	0.753	0.431	**0.769**	**0.695**	0.745	0.417
Ours	0.921	0.893	**0.790**	**0.547**	0.771	0.678	**0.789**	**0.474**	0.746	0.689	**0.773**	**0.422**

on their own or mixed with semantic ones, improves the performance, especially in generalisation. Indeed, we argue that the use of random masks at training time aids the model in detaching the semantic bias interwoven with the task. In fact, while the forgery localisation is highly semantic, it is not guaranteed that the forgeries are produced with the semantics of the scene in mind, differentiating the task from semantic segmentation.

Semantic encoder ablation In our implementation, we chose DINO-v2 primarily due to architectural and resolution compatibility with DepthAnything-v2, which facilitates a more intuitive fusion of features in our cross-attention mechanism, and favourable performance compared to CLIP on self-supervised learning benchmarks requiring semantic understanding [11]. However, CLIP's language supervision may offer rich semantics as well. We conducted an experiment using CLIP (ViT-B/16) instead of DINO-v2, and found that while performance remained reasonable, as shown in Tab. 8, it was slightly lower compared to DINO-v2 in our setup. Importantly, the performance remained competitive with respect to the inference with DepthAnything-v2 only, proving the effectiveness of our novel fusion strategy. Nevertheless, CLIP remains a viable alternative, and we see potential in future exploration of multi-modal supervision within our framework.

C.6 Features and attention analysis

We report in Fig. 7 more examples of the normalised activations of f'_G and f'_S (features before fusion), averaged over channels for tampered inputs. We once again highlight that the spatial distribution of activations is roughly complementary across modalities.

We also report the attention maps, $f_S \leftarrow f_G$ and $f_G \leftarrow f_S$, from the Fusion Block. These attention maps are obtained by averaging the values of the attention over the keys. In particular:

- $f_S \leftarrow f_G$, which is the mean of semantic values over geometry keys, represents which semantic features are actively using geometry features;
- $f_G \leftarrow f_S$, which is the mean of geometry values over semantic keys, represents which geometry features are actively using semantic features.

Also in this case, we observe that the spatial distribution of attention is roughly complementary. Moreover, despite the attention being mostly concentrated in the prediction area, we observe peaks also outside, highlighting that the framework is actively using information from the background as well for the prediction.

C.7 Inference time and memory occupancy

We report in Tab. 9 the inference time per sample in `ms`, the memory occupancy of the forward pass in `GiB` and the input resolution in `px` for each considered method. We remind the reader that we test each method using the suggested resolution in the original papers. For each method, we compute the inference time, from when the sample is available on the GPU to the computation of the localisation

Table 7: **Ablation on the use of semantic and random masks at training time.**

Setup	ID				LoRA				OOD			
	AUC↑	Acc↑	F1↑	IoU↑	AUC↑	Acc↑	F1↑	IoU↑	AUC↑	Acc↑	F1↑	IoU↑
Semantic masks-only	0.965	0.884	**0.805**	0.519	**0.791**	0.609	0.764	0.405	**0.785**	0.656	0.796	0.417
Random masks-only	**0.966**	**0.896**	0.770	0.466	0.781	0.586	0.762	0.400	0.763	0.642	**0.801**	**0.423**
Ours	0.921	0.893	0.790	**0.547**	0.771	**0.678**	**0.789**	**0.474**	0.746	**0.689**	0.773	0.422

Table 8: **RADAR's performance with CLIP as Semantic Encoder.**

Setup	ID				LoRA				OOD			
	AUC↑	Acc↑	F1↑	IoU↑	AUC↑	Acc↑	F1↑	IoU↑	AUC↑	Acc↑	F1↑	IoU↑
CLIP+DA-v2	0.901	0.844	**0.802**	0.503	0.691	0.596	0.758	0.402	0.706	0.627	**0.799**	0.412
DINO-v2+DA-v2 (**Ours**)	**0.921**	**0.893**	0.790	**0.547**	**0.771**	**0.678**	**0.789**	**0.474**	**0.746**	**0.689**	0.773	**0.422**

map, after a GPU warm-up, synchronising all threads before estimating the total inference time. While RADAR is slower than networks trained from scratch, other approaches based on foundation models [45] or LLMs [39] are considerably slower.

As an additional effort to further reduce computational cost, we propose an experiment substituting the DINO-v2 and DepthAnything-v2 backbones with their smaller variants, such as using ViT Small instead of ViT Base. We train this smaller model and compare it using the reduced training protocol described in Sec. 4.4 due to the training times of the full model. This substitution, whose results are depicted in, represents a good trade-off between performance and efficiency. In particular, this variant yields a runtime memory footprint of 3.106 GiB and an inference time of 99.424 ms, representing a 30% reduction in memory and a 57% reduction in inference time compared to the version presented in the main manuscript. Moreover, we are still very competitive in terms of accuracy and localisation compared to baselines in Table 1, even considering the reduced training setup.

In conclusion, RADAR performs competitively in low-resource environments.

C.8 Additional qualitative results

We show in Fig. 8 more qualitative results coming from the commercial inpainters of the BBC-PAIR-OOD split of our benchmark. Moreover, we show in Fig. 9 qualitative results coming from the other datasets of the BBC-PAIR-OOD split, namely CocoGlide, SafireMS-Expert++ and SID-Set. Also, in Fig. 10 we show qualitative results coming from the BBC-PAIR-ID and BBC-PAIR-LoRA splits of our benchmark.

C.9 Detailed quantitative results

We report in Tab. 11, Tab. 13, Tab. 12, Tab. 14 the full results of the evaluation performed in Tab. 1. In Tab. 14 we also show the official result reported from the competitors' papers, highlighting how they are close to our run. We also highlight that SafireMS-Expert++ is in-domain for SAFIRE, as well as SID-Set is in-domain for SIDA. Despite this advantage, we outperform them in the BBC-PAIR-OOD benchmark.

C.10 Additional results on OpenSDI

We report in Tab. 15 additional results on the OpenSDI dataset [82]. Similarly to BBC-PAIR, OpenSDI contains images inpainted employing different diffusion models, but these are only a subset of the one proposed in BBC-PAIR (5 vs. 28), hence, having much less coverage.

D Final remarks

D.1 Limitations

While RADAR achieves state-of-the-art performance in image forgery detection and localisation, several limitations highlight avenues for future work:

https://doi.org/10.52202/085713-1270

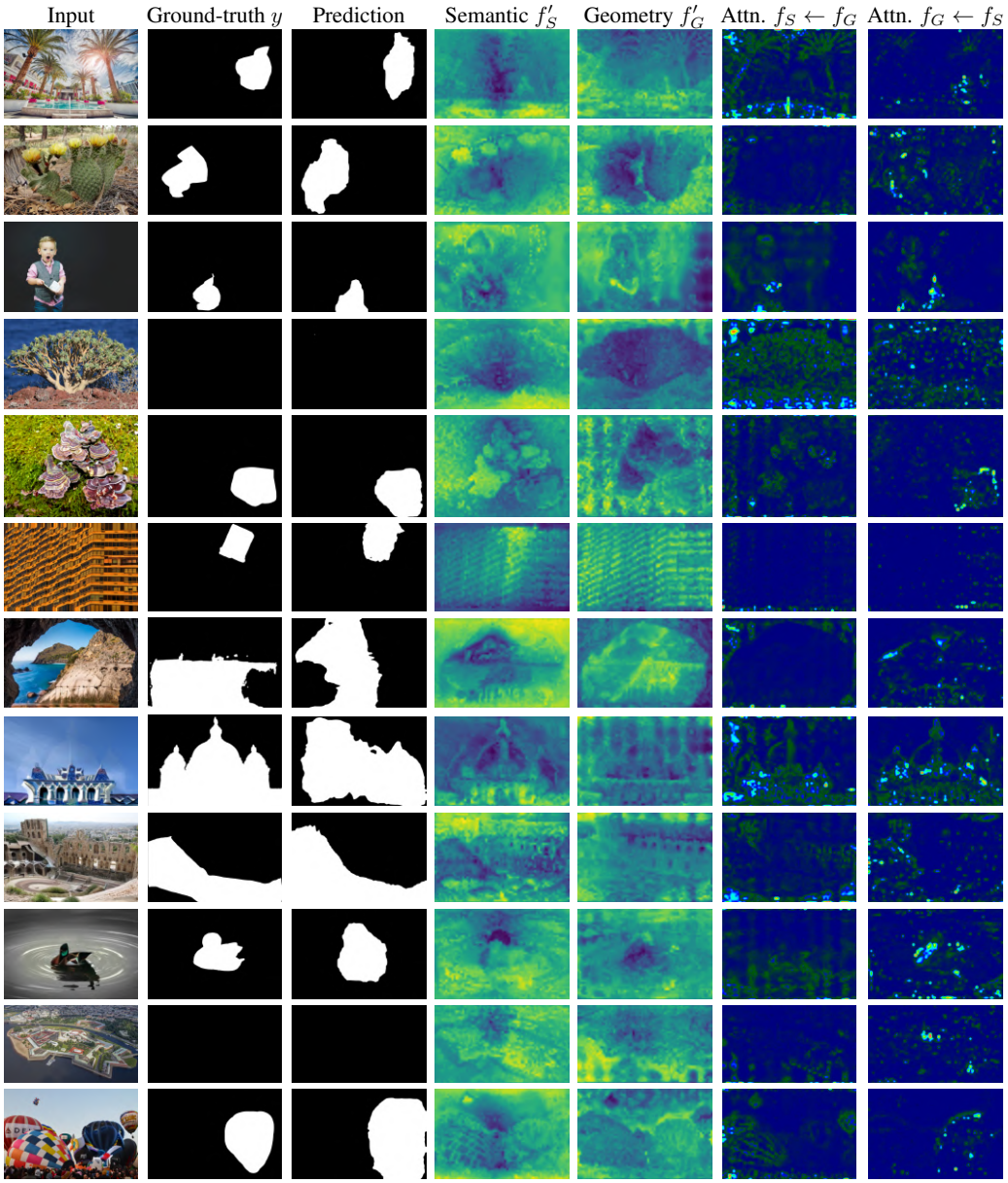


Figure 7: **Features and attention maps.**

Table 9: **Inference time vs. Memory Occupancy vs. Input resolution.**

Property	Ours	HiFi-Net [33]	TruFor [32]	MIML [63]	AdaIFL [48]	Mesorch [94]	SAFIRE [45]	SIDA [39]
Inference time [ms]	228.176	53.852	79.1626	72.920	142.43	41.730	3266.566	725.787
Memory occupancy [GiB]	4.404	5.708	6.187	6.312	9.218	7.611	21.500	15.572
Input resolution [px]	896×896	256×256	512×512	768×768	1024×1024	512×512	1024×1024	1024×1024

1. **Performance gap**: despite outperforming existing methods, our approach still exhibits a non-trivial error rate, particularly in complex forgery scenarios (e.g., unseen inpainters). This suggests significant room for improvement in generalisation and robustness;
2. **Conservative localisation bias**: RADAR tends to prioritise precision over recall in localisation, resulting in fewer false positives at the cost of missed detections. While this aligns with forensic applications where false accusations carry high stakes, it may limit sensitivity in scenarios requiring exhaustive forgery identification;

https://doi.org/10.52202/085713-1270

Table 10: **RADAR's performance in low-resource environments.**

Setup	ID				LoRA				OOD			
	AUC↑	Acc↑	F1↑	IoU↑	AUC↑	Acc↑	F1↑	IoU↑	AUC↑	Acc↑	F1↑	IoU↑
ViT Small	**0.966**	0.892	**0.800**	0.516	0.672	0.549	0.756	0.387	0.731	0.645	**0.787**	0.418
ViT Base (**Ours**)	0.921	**0.893**	0.790	**0.547**	**0.771**	**0.678**	**0.789**	**0.474**	**0.746**	**0.689**	0.773	**0.422**

Table 11: **Full quantitative comparison on BBC-PAIR-ID.**

Method	Stable Diffusion 1.4				Stable Diffusion 1.5				Stable Diffusion 2.1				Stable Diffusion 3				Stable Diffusion 3.5			
	Det.		Loc.		Det.		Loc.		Det.		Loc.		Det.		Loc.		Det.		Loc.	
	AUC↑	Acc↑	F1↑	IoU↑	AUC↑	Acc↑	F1↑	IoU↑	AUC↑	Acc↑	F1↑	IoU↑	AUC↑	Acc↑	F1↑	IoU↑	AUC↑	Acc↑	F1↑	IoU↑
HiFi-Net [33]	0.556	0.500	0.757	0.378	0.636	0.520	0.742	0.372	0.575	0.505	0.754	0.377	0.596	0.505	0.759	0.382	0.653	0.510	0.723	0.362
TruFor [32]	0.657	0.565	0.648	0.361	0.593	0.554	0.691	0.392	0.576	0.544	0.707	0.393	0.543	0.559	0.719	0.417	0.519	0.525	0.778	0.471
MIML [63]	0.511	0.495	0.221	0.114	0.530	0.485	0.211	0.108	0.494	0.505	0.222	0.114	0.449	0.485	0.214	0.110	0.477	0.495	0.210	0.107
AdaIFL [48]	0.561	0.520	0.764	0.383	0.567	0.505	0.762	0.385	0.509	0.505	0.758	0.381	0.595	0.530	0.748	0.377	0.514	0.490	0.764	0.383
Mesorch [94]	0.667	0.610	0.698	0.367	0.568	0.544	0.720	0.379	0.726	0.650	0.744	0.400	0.545	0.545	0.654	0.391	0.536	0.550	0.776	0.424
SAFIRE [45]	0.598	0.530	0.699	0.375	0.597	0.525	0.664	0.381	0.605	0.540	0.672	0.363	0.617	0.535	0.648	0.358	0.625	0.535	0.649	0.370
SIDA [39]	0.590	0.590	0.694	0.460	0.610	0.610	0.800	0.565	0.630	0.630	0.749	0.515	0.615	0.615	0.826	0.573	0.540	0.540	0.690	0.460
RADAR	0.938	0.935	0.813	0.564	0.950	0.935	0.823	0.580	0.939	0.935	0.824	0.580	0.941	0.931	0.825	0.583	0.944	0.929	0.831	0.598

Method	Stable Diffusion XL				Kandinsky 2.2				Kandinsky 3.1				FLUX.1-schnell				FLUX.1-dev			
	Det.		Loc.		Det.		Loc.		Det.		Loc.		Det.		Loc.		Det.		Loc.	
	AUC↑	Acc↑	F1↑	IoU↑	AUC↑	Acc↑	F1↑	IoU↑	AUC↑	Acc↑	F1↑	IoU↑	AUC↑	Acc↑	F1↑	IoU↑	AUC↑	Acc↑	F1↑	IoU↑
HiFi-Net [33]	0.668	0.510	0.726	0.364	0.700	0.510	0.765	0.389	0.624	0.505	0.746	0.373	0.630	0.505	0.770	0.385	0.607	0.515	0.757	0.379
TruFor [32]	0.525	0.520	0.779	0.475	0.499	0.534	0.780	0.473	0.518	0.530	0.757	0.449	0.494	0.510	0.779	0.472	0.558	0.534	0.753	0.432
MIML [63]	0.469	0.485	0.207	0.106	0.469	0.485	0.215	0.110	0.390	0.435	0.219	0.111	0.472	0.490	0.197	0.102	0.419	0.465	0.221	0.113
AdaIFL [48]	0.520	0.475	0.766	0.384	0.506	0.470	0.766	0.384	0.523	0.475	0.765	0.383	0.505	0.505	0.766	0.383	0.531	0.505	0.760	0.383
Mesorch [94]	0.525	0.540	0.780	0.420	0.537	0.545	0.759	0.405	0.550	0.510	0.773	0.402	0.615	0.585	0.763	0.429	0.537	0.520	0.770	0.405
SAFIRE [45]	0.565	0.540	0.634	0.343	0.572	0.520	0.641	0.378	0.559	0.515	0.706	0.404	0.591	0.525	0.708	0.412	0.607	0.540	0.662	0.364
SIDA [39]	0.550	0.550	0.775	0.564	0.735	0.735	0.772	0.558	0.565	0.565	0.783	0.523	0.555	0.555	0.820	0.674	0.590	0.590	0.728	0.465
RADAR	0.946	0.929	0.831	0.598	0.947	0.930	0.840	0.616	0.947	0.930	0.841	0.617	0.949	0.929	0.847	0.630	0.949	0.929	0.847	0.629

3. **Explainability**: although we analyse cross-attention maps and activation patterns to interpret model decisions, the internal reasoning remains opaque. A more intuitive, human-aligned explanation framework would improve trust and usability in critical domains like journalism or law;

4. **Evaluation metrics**: the IFDL field lacks standardised benchmarks and metrics, particularly for localisation granularity (e.g., pixel-wise vs. region-wise accuracy) and real-world robustness. Community-wide efforts to establish unified evaluation protocols would better guide future research.

In future work, we aim to address these limitations by (1) exploring even more expressive architectures to reduce error rates, (2) designing adaptive loss functions to balance precision and recall, (3) integrating post-hoc explainability methods (e.g., concept activation vectors), and (4) collaborating with the IFDL community to define standardized evaluation protocols.

D.2 Broader impact

The development of robust image forgery detection and localisation techniques has significant societal implications. As digital images play a crucial role in journalism, legal evidence, social media, and historical documentation, the ability to reliably detect manipulated content helps combat misinformation, deepfakes, and fraudulent media. This research contributes to the broader effort of ensuring digital media integrity, fostering trust in visual information, and supporting forensic investigations.

However, the deployment of such technologies also raises ethical concerns. Malicious actors could potentially misuse forgery detection models to refine adversarial attacks, making manipulated images even harder to detect. Additionally, false positives in forgery detection could lead to unjust accusations, particularly in sensitive domains like law enforcement or public discourse. To mitigate these risks, it is essential to ensure transparency in model limitations, promote responsible use, and integrate human oversight in critical decision-making processes.

Future advancements in this field should prioritise fairness, avoiding biases that may disproportionately affect certain demographics or media sources. Collaborative efforts between researchers, policymakers, and industry stakeholders will be necessary to establish ethical guidelines and regulatory frameworks for the responsible deployment of image forensics tools.

https://doi.org/10.52202/085713-1270

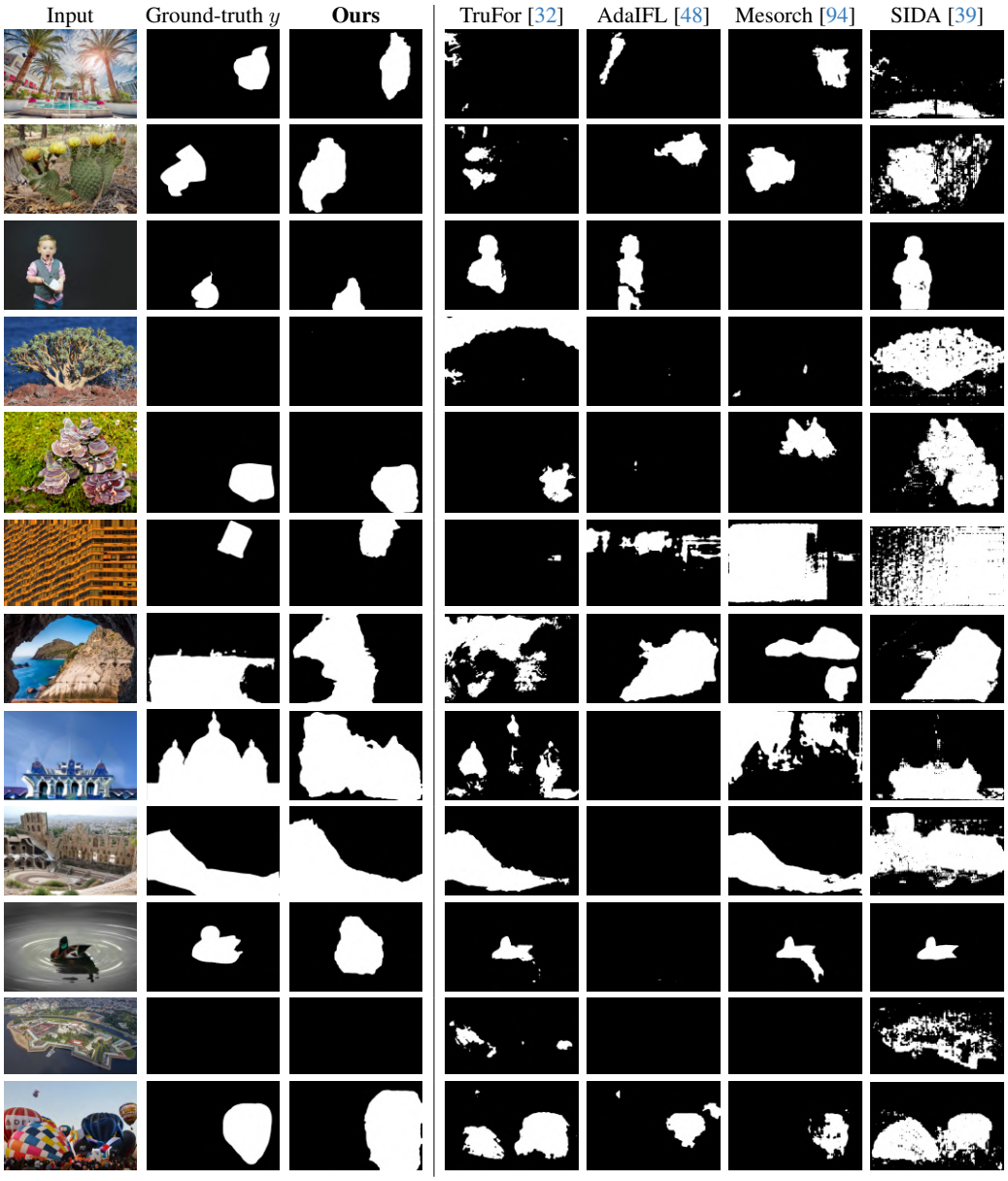


Figure 8: **Qualitative results on BBC-PAIR-OOD (closed-source inpainters).**

By advancing the state of the art in forgery detection, this work not only enhances media authenticity but also encourages further research into trustworthy multimedia systems, ultimately benefiting society at large.

D.3 Safeguards

Due to the nature of the topic, the proposed method may be vulnerable to malicious exploitation, such as adversarial attacks designed to produce even more convincing image tampering that can evade IFDL techniques. To mitigate this risk, users will be required to follow specific usage guidelines when accessing both the training data and the trained models.

Furthermore, all images in the dataset will include C2PA metadata to facilitate usage tracking. When a user accesses the dataset, C2PA metadata will automatically record the user's name and affiliated institution in the manifest, thereby promoting transparency and fair use. If the C2PA metadata is

Table 12: **Full quantitative comparison on BBC-PAIR-LoRA.**

Method	dAIversity Detailer 1.5				dAIversity SD3.5-LoRA				Flux-Detailer-LoRA				Dreamshaper SDXL-1-0				Juggernaut-XL-v6			
	Det.		Loc.		Det.		Loc.		Det.		Loc.		Det.		Loc.		Det.		Loc.	
	AUC↑	Acc↑	F1↑	IoU↑	AUC↑	Acc↑	F1↑	IoU↑	AUC↑	Acc↑	F1↑	IoU↑	AUC↑	Acc↑	F1↑	IoU↑	AUC↑	Acc↑	F1↑	IoU↑
HiFi-Net [33]	0.622	0.500	0.739	0.369	0.756	0.510	0.708	0.355	0.659	0.500	0.772	0.365	0.603	0.500	0.736	0.368	0.614	0.500	0.731	0.366
TruFor [32]	0.510	0.520	0.760	0.424	0.516	0.550	0.772	0.469	0.573	0.530	0.771	0.456	0.498	0.530	0.765	0.448	0.490	0.520	0.773	0.459
MIML [63]	0.520	0.500	0.228	0.133	0.577	0.510	0.242	0.135	0.531	0.500	0.244	0.125	0.554	0.520	0.251	0.146	0.509	0.530	0.244	0.136
AdaIFL [48]	0.514	0.500	0.759	0.399	0.526	0.500	0.761	0.414	0.549	0.540	0.759	0.408	0.588	0.580	0.784	0.452	0.510	0.530	0.761	0.403
Mesorch [94]	0.594	0.530	0.763	0.406	0.536	0.510	0.753	0.389	0.549	0.490	0.753	0.399	0.627	0.560	0.758	0.402	0.542	0.520	0.757	0.393
SAFIRE [45]	0.500	0.490	0.676	0.399	0.528	0.490	0.676	0.399	0.528	0.540	0.681	0.396	0.572	0.530	0.652	0.384	0.492	0.490	0.709	0.424
SIDA [39]	0.520	0.520	0.744	0.539	0.540	0.540	0.806	0.660	0.510	0.510	0.219	0.107	0.570	0.570	0.768	0.538	0.600	0.600	0.852	0.636
RADAR	0.944	0.840	0.821	0.547	0.930	0.820	0.820	0.552	0.891	0.770	0.808	0.523	0.892	0.760	0.807	0.513	0.895	0.760	0.807	0.513

Method	Perfection 1.5				Perfection Flux				flux-RealismLora				ReaPhoLoRA 1.5				Yamer's Realsim-v2 XL			
	Det.		Loc.		Det.		Loc.		Det.		Loc.		Det.		Loc.		Det.		Loc.	
	AUC↑	Acc↑	F1↑	IoU↑	AUC↑	Acc↑	F1↑	IoU↑	AUC↑	Acc↑	F1↑	IoU↑	AUC↑	Acc↑	F1↑	IoU↑	AUC↑	Acc↑	F1↑	IoU↑
HiFi-Net [33]	0.642	0.500	0.732	0.366	0.666	0.510	0.711	0.361	0.674	0.510	0.720	0.362	0.664	0.500	0.731	0.366	0.602	0.500	0.741	0.370
TruFor [32]	0.502	0.530	0.746	0.407	0.535	0.520	0.762	0.433	0.560	0.540	0.765	0.442	0.499	0.530	0.756	0.426	0.505	0.520	0.776	0.470
MIML [63]	0.473	0.480	0.224	0.120	0.507	0.490	0.244	0.124	0.507	0.500	0.244	0.124	0.489	0.459	0.234	0.134	0.503	0.510	0.241	0.137
AdaIFL [48]	0.498	0.500	0.755	0.391	0.570	0.560	0.756	0.405	0.577	0.570	0.760	0.406	0.532	0.490	0.758	0.408	0.538	0.550	0.777	0.434
Mesorch [94]	0.554	0.520	0.764	0.399	0.549	0.540	0.753	0.400	0.563	0.530	0.755	0.393	0.556	0.530	0.760	0.400	0.533	0.460	0.761	0.399
SAFIRE [45]	0.510	0.530	0.641	0.363	0.469	0.510	0.657	0.374	0.502	0.530	0.679	0.416	0.531	0.520	0.663	0.378	0.513	0.520	0.700	0.417
SIDA [39]	0.550	0.550	0.696	0.477	0.530	0.530	0.957	0.822	0.520	0.520	0.210	0.111	0.610	0.610	0.663	0.509	0.590	0.590	0.888	0.685
RADAR	0.903	0.771	0.808	0.516	0.892	0.755	0.806	0.511	0.882	0.743	0.803	0.504	0.892	0.758	0.810	0.517	0.893	0.756	0.809	0.515

Table 13: **Full quantitative comparison on BBC-PAIR-Commercial.**

Method	ClipDrop				Dall-E 2				Adobe Firefly				FLUX.1 Fill [pro]			
	Det.		Loc.		Det.		Loc.		Det.		Loc.		Det.		Loc.	
	AUC↑	Acc↑	F1↑	IoU↑	AUC↑	Acc↑	F1↑	IoU↑	AUC↑	Acc↑	F1↑	IoU↑	AUC↑	Acc↑	F1↑	IoU↑
HiFi-Net [33]	0.344	0.500	0.815	0.413	0.582	0.513	0.675	0.399	0.531	0.513	0.750	0.405	0.372	0.500	0.773	0.413
TruFor [32]	0.605	0.546	0.800	0.481	0.563	0.520	0.757	0.418	0.499	0.493	0.780	0.419	0.442	0.500	0.762	0.419
MIML [63]	0.704	0.500	0.178	0.096	0.571	0.493	0.184	0.097	0.528	0.500	0.186	0.098	0.561	0.500	0.184	0.097
AdaIFL [48]	0.518	0.513	0.804	0.421	0.522	0.506	0.805	0.422	0.500	0.513	0.809	0.424	0.468	0.460	0.810	0.422
Mesorch [94]	0.572	0.526	0.818	0.433	0.562	0.553	0.811	0.419	0.521	0.540	0.813	0.412	0.527	0.553	0.806	0.417
SAFIRE [45]	0.422	0.493	0.674	0.368	0.526	0.500	0.702	0.369	0.513	0.506	0.685	0.396	0.424	0.500	0.673	0.405
SIDA [39]	0.493	0.493	0.696	0.411	0.486	0.486	0.695	0.396	0.546	0.546	0.703	0.409	0.513	0.513	0.709	0.412
RADAR	0.682	0.620	0.804	0.430	0.685	0.586	0.800	0.420	0.642	0.555	0.806	0.420	0.638	0.550	0.808	0.422

Method	Ideogram				LightX				Phot.AI				YouCam			
	Det.		Loc.		Det.		Loc.		Det.		Loc.		Det.		Loc.	
	AUC↑	Acc↑	F1↑	IoU↑	AUC↑	Acc↑	F1↑	IoU↑	AUC↑	Acc↑	F1↑	IoU↑	AUC↑	Acc↑	F1↑	IoU↑
HiFi-Net [33]	0.374	0.500	0.764	0.413	0.460	0.500	0.806	0.413	0.320	0.500	0.799	0.414	0.388	0.500	0.815	0.411
TruFor [32]	0.476	0.513	0.805	0.419	0.663	0.580	0.761	0.470	0.507	0.533	0.825	0.450	0.462	0.493	0.746	0.394
MIML [63]	0.501	0.493	0.188	0.099	0.823	0.506	0.165	0.091	0.634	0.500	0.166	0.088	0.694	0.500	0.194	0.101
AdaIFL [48]	0.483	0.493	0.804	0.413	0.580	0.573	0.787	0.413	0.491	0.506	0.809	0.422	0.452	0.460	0.803	0.412
Mesorch [94]	0.526	0.526	0.807	0.406	0.782	0.706	0.809	0.495	0.593	0.573	0.808	0.422	0.525	0.526	0.801	0.403
SAFIRE [45]	0.447	0.486	0.690	0.371	0.584	0.506	0.647	0.395	0.468	0.500	0.693	0.428	0.537	0.500	0.722	0.428
SIDA [39]	0.493	0.493	0.714	0.418	0.553	0.553	0.695	0.404	0.546	0.546	0.711	0.415	0.486	0.486	0.685	0.374
RADAR	0.623	0.538	0.810	0.421	0.638	0.554	0.805	0.421	0.642	0.556	0.805	0.421	0.639	0.553	0.804	0.420

removed, a hash-based verification mechanism will be provided: users can query a list of hashes to determine whether a suspicious image originated from the dataset.

Finally, while efforts have been made to filter sensitive content, there is no absolute guarantee that NSFW (Not Safe For Work) images have not been generated during the inpainting process. To help mitigate this risk, all images have been analysed using the default Stability AI safety checker, both before and after inpainting. Relevant flags are included in the dataset's metadata, allowing users to filter out potentially inappropriate content if desired.

https://doi.org/10.52202/085713-1270

Table 14: **Full quantitative comparison on BBC-PAIR-OOD.** Official results from original paper marked in blue.

Method	BBC-PAIR-Comm				CocoGlide				SID-Set				SafireMS-Expert++			
	Det.		Loc.		Det.		Loc.		Det.		Loc.		Det.		Loc.	
	AUC↑	Acc↑	F1↑	IoU↑	AUC↑	Acc↑	F1↑	IoU↑	AUC↑	Acc↑	F1↑	IoU↑	AUC↑	Acc↑	F1↑	IoU↑
HiFi-Net [33]	0.421	0.503	0.775	0.410	0.632	0.534	0.519	0.343	0.518	0.503	0.843	0.463	0.726	0.558	0.620	0.313
TruFor [32]	0.527	0.522	0.780	0.434	0.752	0.647	0.711	0.381	0.460	0.514	0.907	0.467	0.700	0.635	0.610	0.467
					0.752	0.639	0.720	N.A.								
MIML [63]	0.627	0.499	0.181	0.096	0.763	0.664	0.276	0.147	0.280	0.303	0.077	0.040	0.845	0.552	0.214	0.111
AdaIFL [48]	0.502	0.503	0.804	0.419	0.555	0.535	0.701	0.376	0.534	0.514	0.909	0.466	0.832	0.665	0.749	0.527
Mesorch [94]	0.576	0.563	0.809	0.426	0.727	0.640	0.704	0.374	0.567	0.525	0.920	0.468	0.797	0.711	0.727	0.498
SAFIRE [45]	0.490	0.499	0.686	0.395	0.557	0.519	0.647	0.359	0.510	0.500	0.784	0.407	0.814	0.509	0.747	0.596
					N.A.	N.A.	0.635	N.A.								
SIDA [39]	0.515	0.515	0.701	0.405	0.625	0.625	0.650	0.376	0.915	0.915	0.842	0.444	0.662	0.662	0.692	0.476
									N.A.	0.901	0.739	0.438				
RADAR	0.649	0.564	0.805	0.422	0.707	0.654	0.670	0.381	0.932	0.796	0.861	0.453	0.932	0.821	0.802	0.545

Table 15: **Full quantitative comparison on OpenSDI.**

Method	Det.		Loc.	
	AUC↑	Acc↑	F1↑	IoU↑
RADAR	**0.684**	**0.564**	0.865	**0.614**
SIDA	0.536	0.536	0.735	0.394
SAFIRE	0.476	0.506	0.724	0.383
Mesorch	0.549	0.526	0.826	0.434
AdaIFL	0.490	0.481	**0.889**	0.540
MIML	0.590	0.529	0.091	0.046
TruFor	0.552	0.525	0.848	0.454
HiFi-Net	0.496	0.499	0.831	0.415

https://doi.org/10.52202/085713-1270



Figure 9: **Qualitative results on other BBC-PAIR-OOD benchmarks.**

https://doi.org/10.52202/085713-1270

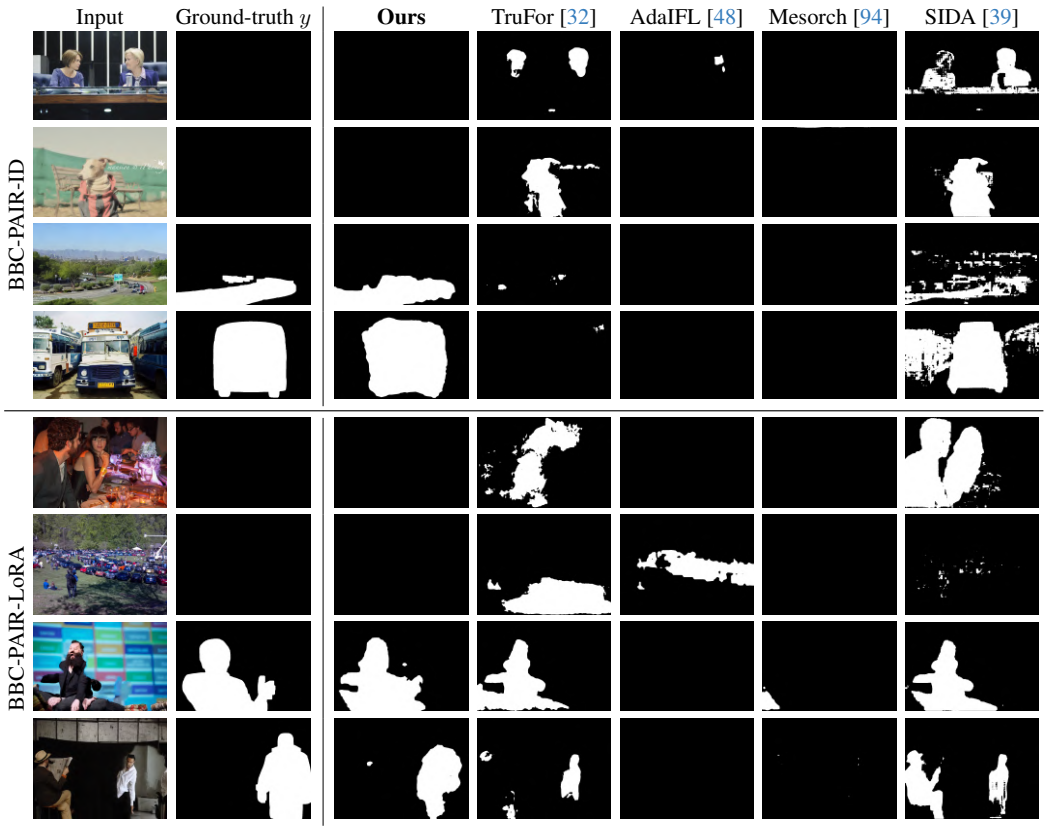


Figure 10: **Qualitative results BBC-PAIR-ID and BBC-PAIR-LoRA benchmarks.**

https://doi.org/10.52202/085713-1270